國立臺灣大學電機資訊學院光電工程學研究所

碩士論文

Graduate Institute of Photonics and Optoeletronics

College of Electrical Engineering and Computer Science

National Taiwan University

Master Thesis

使用矽核光纖製作具有高品質因子迴音廊模態之矽微米球共

振腔

Fabrication of Si Microsphere Resonators with High Q

Whispering Gallery Modes by Using Si-cored Fibers

林哲安

Che-An Lin

指導教授：王倫 博士

Advisor: Lon A. Wang, Ph.D.

中華民國 104 年 2 月

February, 2015

國立臺灣大學碩士學位論文
口試委員會審定書

利用矽核光纖製作具有高品質因子迴音廊模態
之矽微米球共振腔
Fabrication of Si Microsphere Resonators with
High Q WGM by Using Si-Cored Fibers

本論文係林哲安君（學號 R01941085）在國立臺灣大學
光電工程學研究所完成之碩士學位論文，於民國 104 年 2 月
2 日承下列考試委員審查通過及口試及格，特此證明

口試委員：

_____王倫_____（指導教授）

胡振國　　　　毛明華

所　長　林恭如

誌謝

中文摘要

在本論文中，我們將粉末套管法與垂直下拉法做結合來製作單晶矽核光纖 (silicon-cored fibers)。我們使用成本便宜許多的多晶矽粉來取代成本高昂的單晶矽棒或晶種來製作矽核光纖。藉由優化抽絲的相關參數後，可以成功製作出長度長達一公尺的單晶矽核光纖，也因為是單晶的原因，其傳輸損耗可以被降低到小於世界上其他的團隊。最後抽出來的矽核光纖其尺寸約為玻璃包覆層直徑 100-300 微米、矽核心直徑 10-30 微米。

我們根據先前製作玻璃微光纖的經驗與玻璃光纖抽絲系統來對矽核光纖做二次抽絲，並成功的製作出矽核錐狀光纖(silicon-cored tapered fiber)。使用氫氧焰當作熱源與電動馬達來當作移動源。已成功將一個原先尺寸為矽核心直徑 20 微米抽細到矽核心直徑 2.6 微米。

我們採用二氧化碳雷射來加熱矽核光纖中裸露的矽核心來快速製備具有高品質因子(quality factor)迴音廊模態(whispering gallery modes)的矽微米球共振腔 (silicon microsphere resonator)。使用玻璃錐狀光纖耦合法來激發在矽微米球上的迴音廊模態，得到的最高品質因子為 4×10^5。本文中，也藉由熱光效應(thermo-optic effect)來探討關於在矽材料上的共振波長飄移現象。

關鍵字:矽核光纖、矽微米球共振腔、迴音廊模態、高品質因子

ABSTRACT
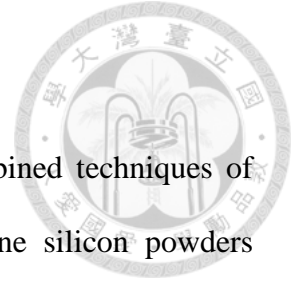
Single-crystal silicon-cored fibers were made by using a combined techniques of powder-in-tube and vertical-drawing. Much cheaper polycrystalline silicon powders substituting expensive single-crystal silicon powders or seed rods were packed into a fused silica tube. By optimizing the drawing parameters, meter-long silicon-cored fibers were obtained with ultralow transmission losses because the entire lengths of silicon cores were single crystalline. The Si-cored fibers were drawn with resultant silica cladding and Si core diameters being in the range of 100-300 μm and 10-30 μm, respectively.

We also demonstrated a fiber drawing system for fabricating Si cored tapered fiber. A fiber drawing system equipped with oxy-hydrogen flame and transition stage was used. According to the previously accumulated knowledge in fabrication of silica microfiber, we successfully fabricated Si cored tapered fibers with diameter of 2.6 μm in the waist section from an original Si-cored fiber with diameter of 20 μm.

Silicon microsphere resonators which exhibited high quality factor (Q) whispering-gallery-modes (WGMs) could be rapidly fabricated from Si-cored fibers using CO_2 laser reformation. WGMs were excited by using the tapered silica fiber coupling technique, and a record resonant Q as high as 4×10^5 was obtained. The shift of resonant wavelength caused by thermo-optic effect of Si material was also observed.

Keywords: silicon-cored fiber, silicon microsphere resonator, whispering gallery modes, high quality factor
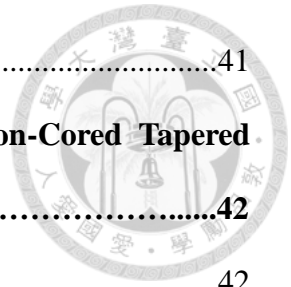
Statement of Contributions

1. Optimizing Si-cored fibers with smaller dimension and higher throughput.

2. Demonstration to fabrication of Si-cored tapered fibers, including fabrication setup and optical characterization.

3. Building up measurement system of WGM, including system setup, coupling technique and optical characterization.

4. Fabrication and measurement of Si microsphere WGM resonator by using CO_2 laser reformation.

CONTENTS

References   88

LIST OF FIGURES

ix

LIST OF TABLES

Chapter 1　Introduction

1.1　Motivation

Over the past few decades, silicon (Si) plays a dominant role in the microelectronics industry due to its ever lowering cost per bit, the second most abundant element on earth and well-known material for producing electronics devices. In addition to be mainly applied to microelectronics industry, Si photonics [1] attracts more attention and has been intensively studied in recent years, because the electrical interconnections for electron are not sufficient to meet the dramatically increased amount of information. Hence, replacing the electrical interconnections by optical interconnections could provide a solution for high bandwidth, high speed and large capacity.

Recently, a novel concept about the combination of Si materials and fiber optics was firstly proposed and demonstrated by using high-pressure chemical vapor deposition method by Sazio et al. in 2006 at University of Southampton/Pennsylvania State University [2], and have become an emerging research topics. Compared to traditional optical fibers made all from silica materials, such combination of semiconductor core and dielectric cladding provide a possibility for the manipulation of both photons and electrons due to the fiber optics structures and semiconductor properties [3, 4]. This concept of Si-cored fibers can provides a variety of applications in nonlinear optics, sensing and modulation [5]. Based on our experience accumulated for past years in silica optical fibers, we decided to fabricate our own Si-cored fibers by adopting molten core drawing method and look forward to finding applications in the fields of photonics and electronics.

In the last decade, the resonators exhibiting Whispering Gallery Modes (WGMs) have

been intensively investigated [6-8] because of their unique spectral features including high quality factors (Q), small mode volume, size-dependent resonance and convenient light coupling. WGM-resonators reported in the past are mostly based on silica materials in different shapes such as microsphere [9], microdisk [10] and microtoroid [11], and could be found in various applications, for example, bio-sensing [12], microlasing [13] and filtering [14]. A schematic diagram of a WGMs microsphere resonator through a silica tapered fiber coupling is shown in Fig. 1-1. Compared to the silica materials, Si materials could provide great potential applications, for example its Raman gain coefficient is four orders of magnitude higher than that in silica [15]. In addition, Si could even be applied for sensing and power delivery at near- and mid- infrared region (λ= 1.1-6.7 μm) due to Si's boarder transparency window, however, silica's transparency window (λ= 0.2-2.1 μm) is too narrow to achieve that. Therefore, for working in such wavelength region, it is desirable to have Si-based high-Q resonators. So far Si WGM-resonators in different shapes, such as microdisk [16], microring [17] microcylindrical [18] and microsphere [19, 20] have been reported in the past and become a possible material choice for optoelectronics devices. It's noted that to obtain a 3-dimensional microsphere is relatively difficult be formed by using a standard semiconductor process. Hence, we present a method to form a microsphere by adopting CO_2 laser exposure in this thesis. To the best of our knowledge, such Si microsphere resonator fabricated by using laser reformation method with high Q was first time to be reported.
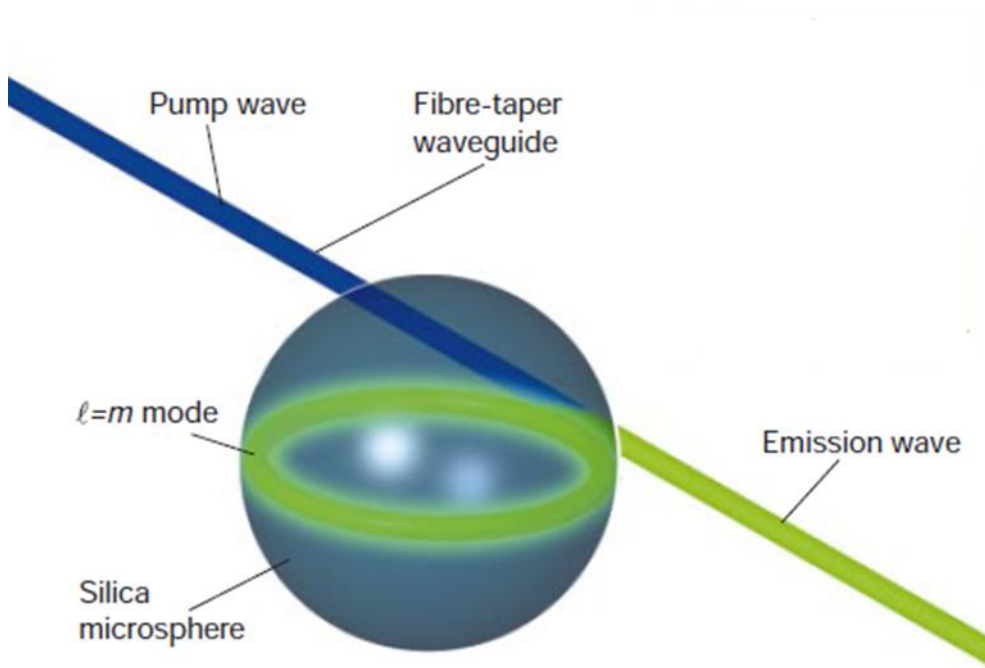
Fig. 1-1 Illustration of a WGM silica microsphere resonators through a tapered fiber coupling [8].

1.2 Literature Review

1.2.1 Fabrication Methods of Silicon-Cored Fibers

The concept about deposition of semiconductor by using chemical vapor deposition method was firstly proposed and published on *Science* in 2006 by Sazio et al. at University of Southampton and Pennsylvania State University [2]. This report opened a new vision on the combination of fiber optics and semiconductor materials. Their Si-cored fibers are fabricated using a high pressure microfluidic chemical deposition technique in which precursors are configured to flow down a silica capillary at high temperatures. This way can definitely provide amorphous silicon core with high quality, but it is a time-consuming and expensive process and difficult to have high throughput. Their Si-cored fibers have a transmission loss of ~5dB/cm at 1.55 μm with a ~5.6 μm amorphous core diameter [18].

Another group, Ballato et al., at Clemson University, they used the molten core method to fabricate Si-cored fibers and published in *Optics Express* in 2008 [21]. A single-crystal Si rod made by Czochralski method was inserted into an end-sealed silica tube preform for assembling. Fibers were drawn using the draw tower at temperatures conventionally used for fabricating telecommunications-grade silica fiber (approximately 1950 ° C). Approximately 30 m of fiber was drawn, but the air bubble density was high, so they selected several approximately 5 cm bubble-free length for experiment. The cross-section view of Si-cored fiber is shown in Fig. 1-2. Their fibers showed a propagation losses of 2.7 dB/cm at wavelength of 1.306 μm with a core diameter of 50 μm.
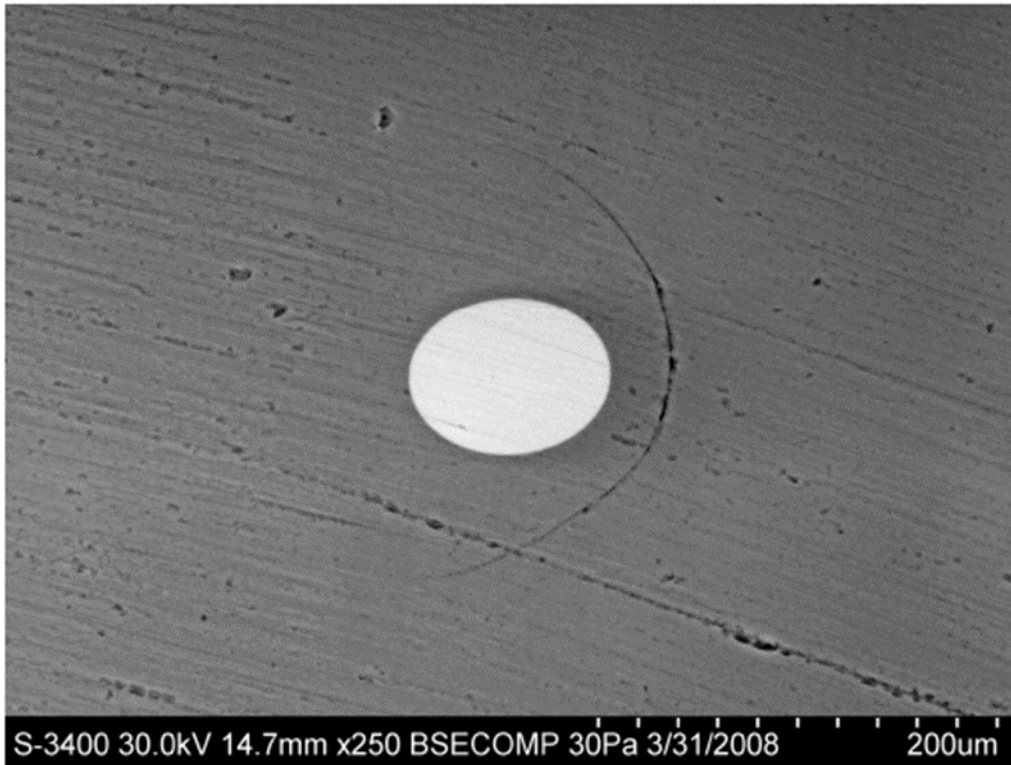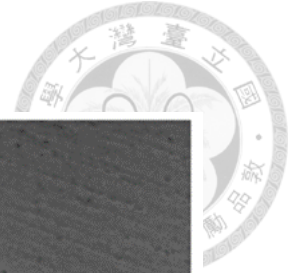
Fig. 1-2 Scanning electron micrograph image of the core region of the Si core, silica cladding optical fiber [21].

B. Scott's group at Virginia Polytechnic Institute and State University also proposed the molten core drawing method to fabricate Si-cored fiber, but they used the single-crystal powders to substitute single-crystal rod in the horizontal drawing system illustrated in Fig. 1-3 to make polycrystalline Si-cored fibers with cladding diameters ranging from 40 to 240 μm and core diameters from 10 to 100 μm, an overall length of fiber are approximately 7 cm [22]. Their transmission spectrum of Si-cored fiber compared to multi-mode silica fiber is shown in Fig. 1-4.
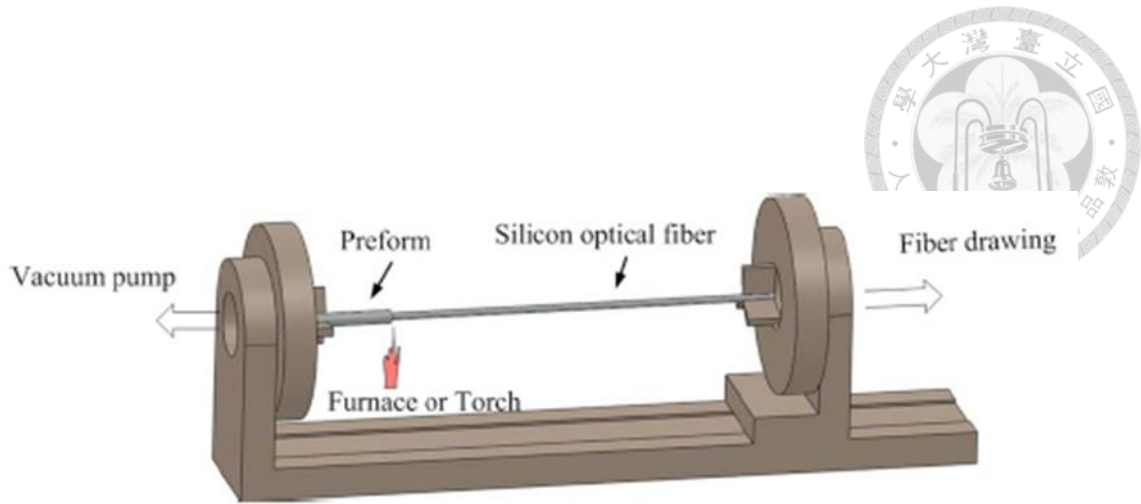
Fig. 1-3 Illustration of the horizontal fiber drawing system [22].
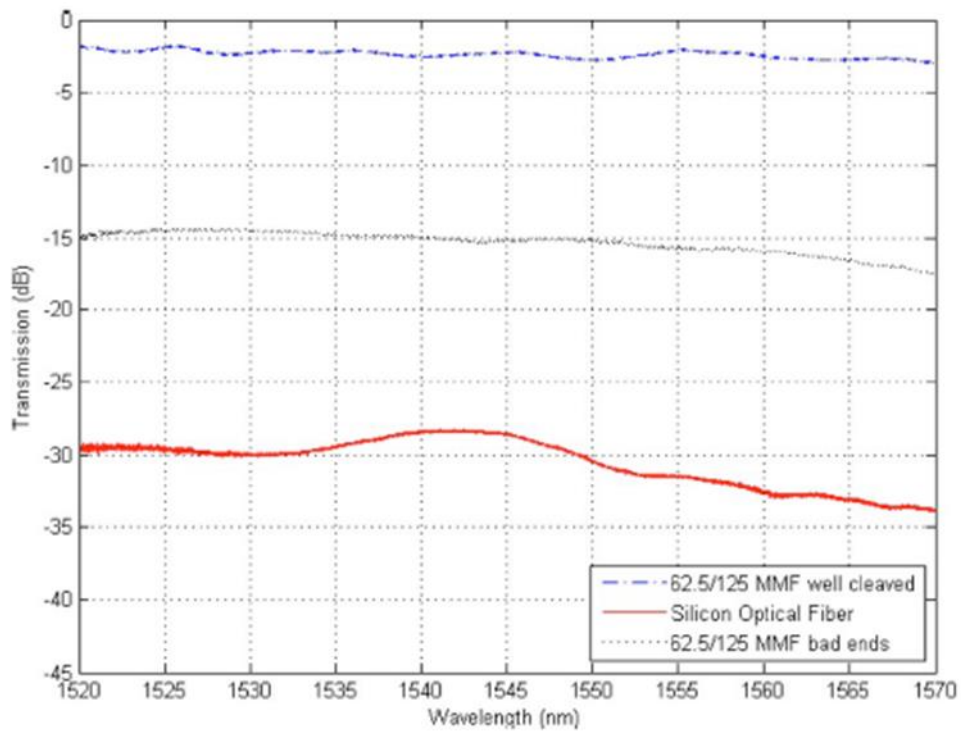
Fig. 1-4 Optical transmission spectrum of a well-cleaved MMF, Si-cored fiber and an uncleaved MMF. [22].

1.2.2 Silicon-Based Whispering Gallery Modes Resonators

WGM-resonators reported in the past are mostly based on silica materials, but there are more and more reports with respect to Si-based WGM resonators in the past decade. The microdisk structure in Si material was published on Optics Express in 2007. This report demonstrated the fabrication and experimental characterization of an ultra-high Q Si microdisk resonator. A planar Si microdisk resonator with ultra-high Q (~3 x 10^6) was fabricated on a silicon-on-insulator (SOI) substrate whose pattern was defined by electron-beam lithography and followed by two-step etching process for realization, the SEM picture and transmission spectrum with WGMs resonance are shown in Fig. 1-5 and Fig. 1-6 [16], respectively.
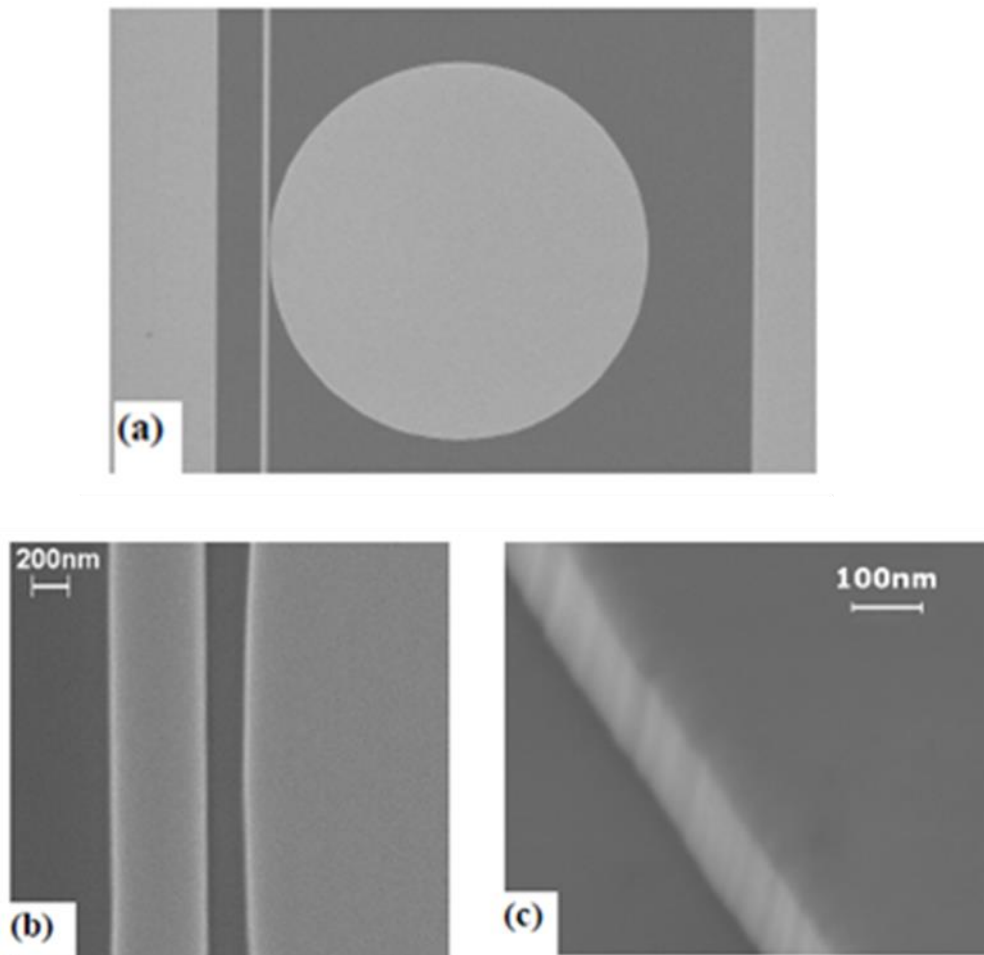
Fig. 1-5 (a) SEM micrograph of a Si microdisk resonator side-coupled to a waveguide; the disk radius is 20 μm and its thickness is 225 nm. The waveguide width is 550 nm and the gap between the disk and the waveguide is 220 nm. (b) A closer view of the structure at the waveguide-cavity coupling region. (c) Sidewall of the microdisk captured at an azimuth angle 30° and sample tilt angle 30° [16].
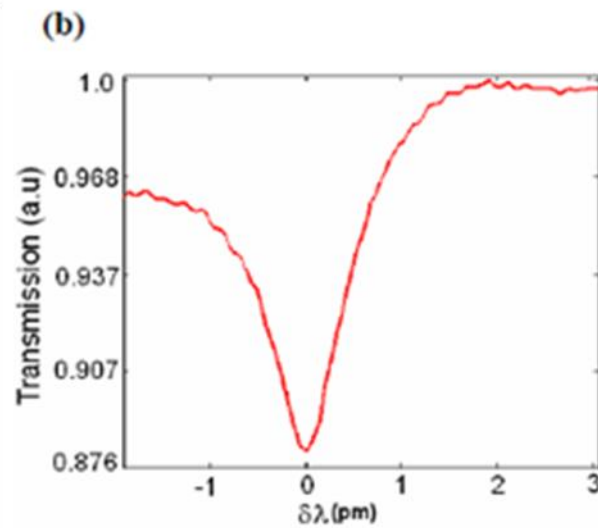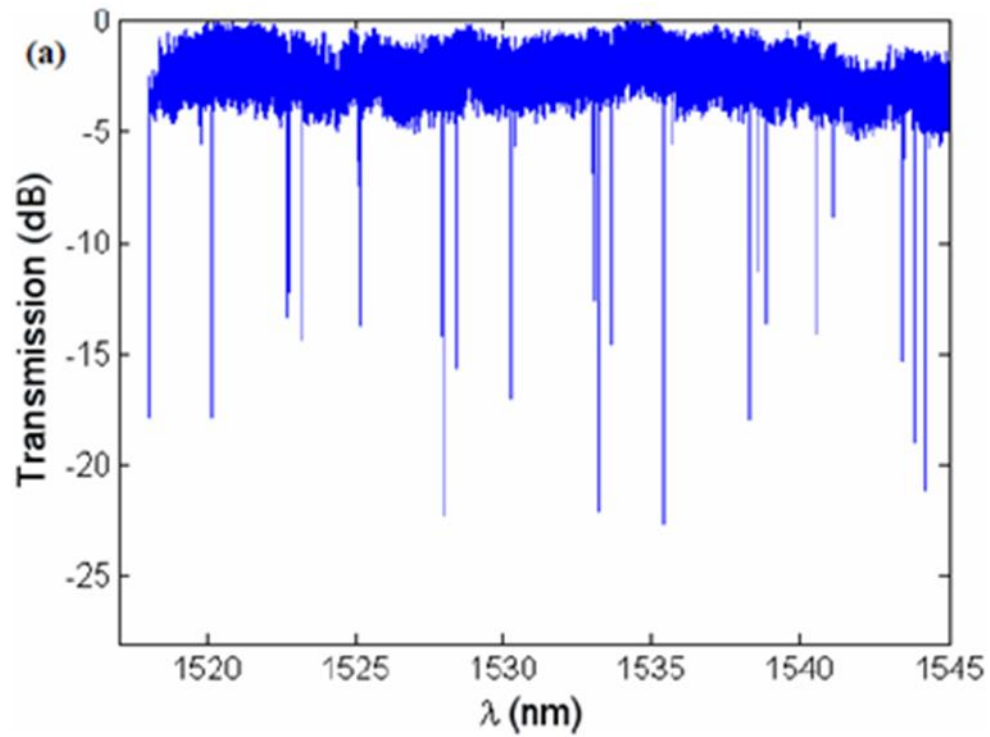
Fig. 1-6 (a) Spectrum of the microdisk resonator for TE polarization. (b) An ultra-high Q=2 x 10^6 was observed at λ=1520.188 nm [16].

In 2010, a Si microring resonator applied for sensing with sharp asymmetrical resonance by end face reflection structure was reported by Yi et al. in *Optics Express*. This disk resonator is also fabricated by standard semiconductor process on an SOI substrate, pattered by e-beam lithography, etched by reactive ion etching, the schematics diagram is shown in Fig. 1-7. A high Q (~3.8 x 10^4) was achieved and applied for chemical sensing [17].
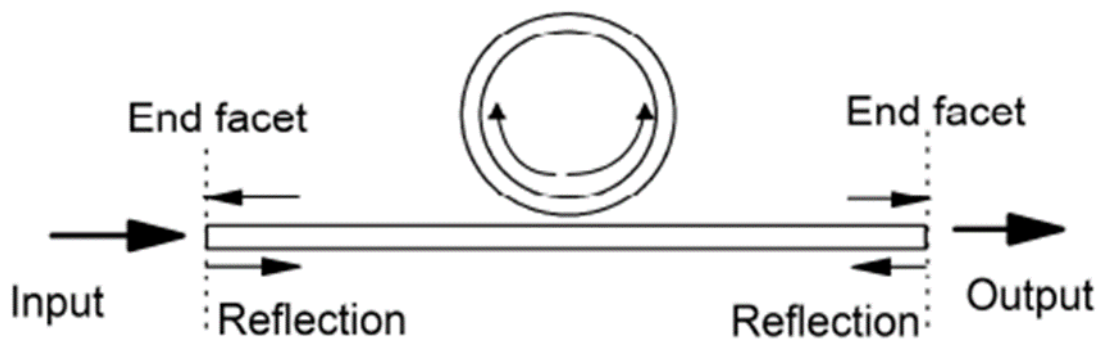
Fig. 1-7 Schematic diagram of microring resonator with end facet reflection structure [17].

A Si microcylindrical resonator was fabricated from Si-cored fiber as well in 2011 on *Applied Physics Letters*. The Si-cored fiber in this work was fabricated by the high pressure chemical vapor deposition technique [2]. The silica cladding of Si-cored fiber was removed by buffered hydrofluoric acid in the first, then the released Si-core became a microcylindrical resonator directly. The tapered fiber coupling method was used to excite WGMs. A high Q (~2.8 x 10^4) was obtained at wavelength of 1.547 μm with 17 dB extinction ratio, the SEM image and resonant spectrum are shown in Fig. 1-8 [18].
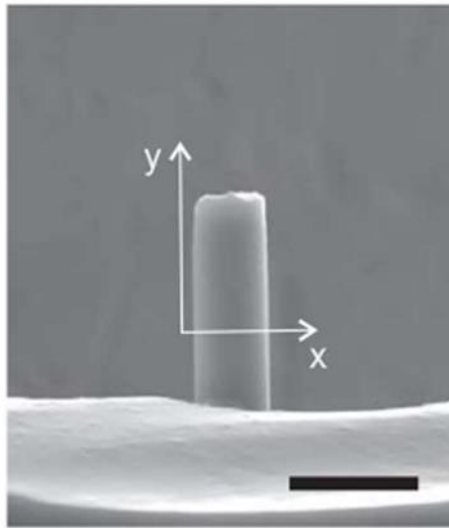
(a)
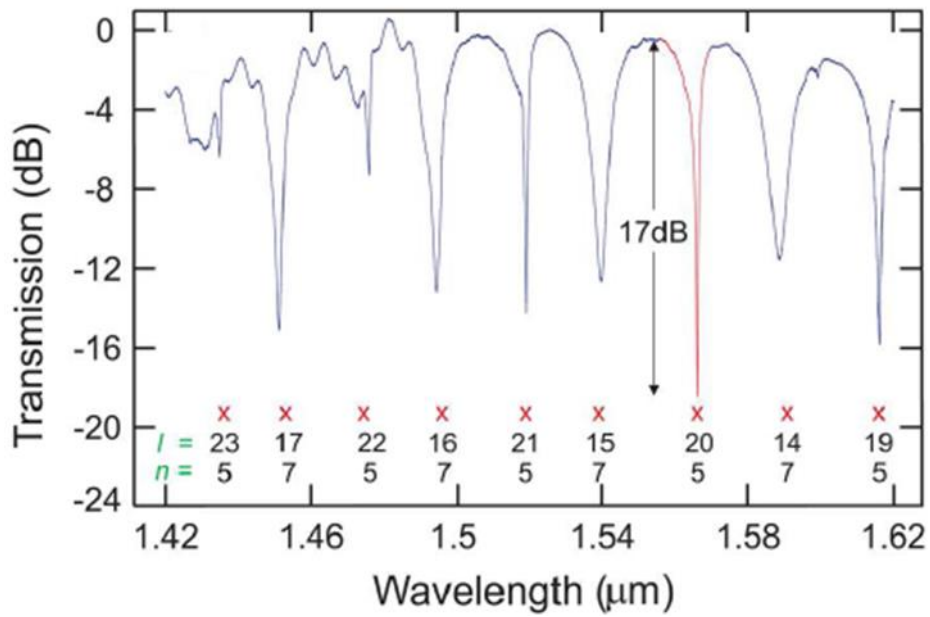
(b)

Fig. 1-8 (a) SEM image of a released Si microcylindrical resonator in diameter of 5.6 μm, scale bar 10 μm. (b) Transmission spectrum with labeled modes, the resonant dip with 17 dB extinction ratio loaded the highest Q~2.8 x 10⁴ [18].

Ali's team have investigated Si microsphere resonator before our work is in Koç University, Istanbul, Turkey. It's worth noting that their microsphere was produced by solidification of molten Si melt [23]. This free-fall solidification process through a plasma furnace from a molten Si melt, the Si in liquid phase would dropped from the top and gradually became into sphere shape via the surface tension during the period of free-fall. A high-Q (~2 x 10^5) isolated Si microsphere in diameter of 530 μm was obtained and had been applied for optical modulation, the Si microscope image and transmission spectrum are shown in Fig. 1-9 and Fig. 1-10.
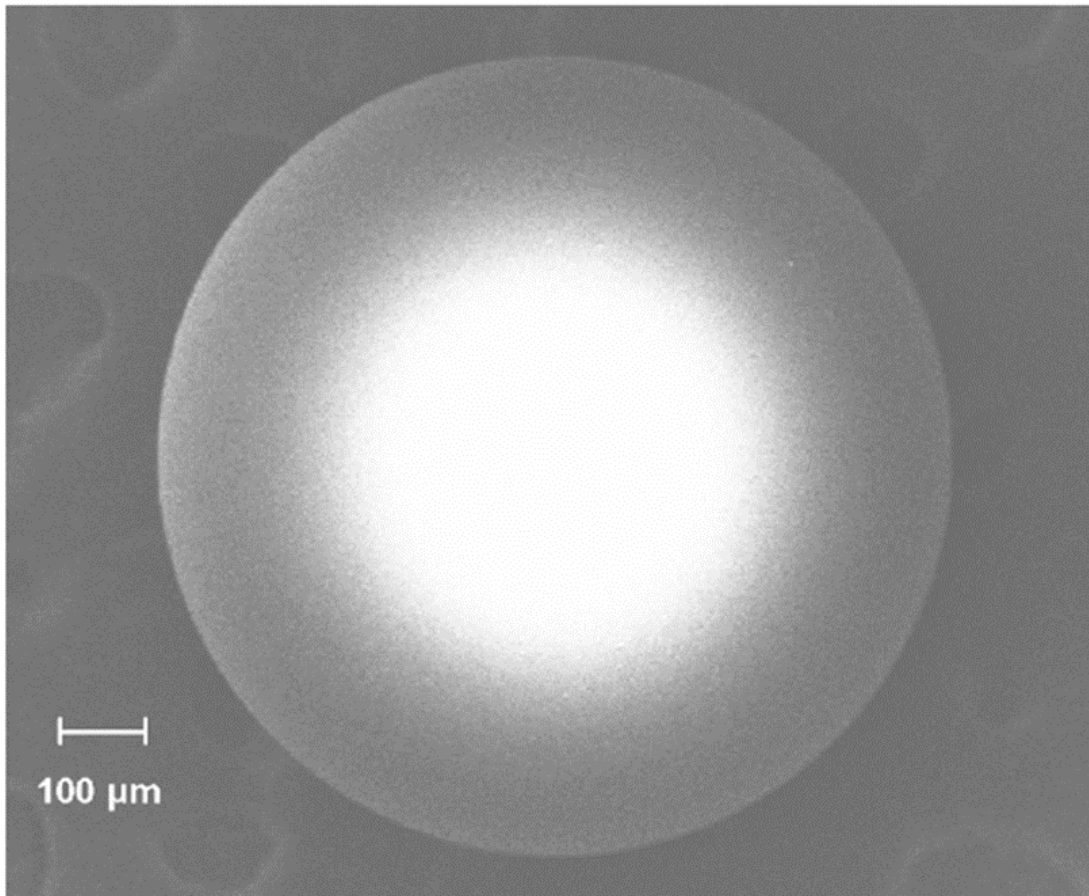
Fig. 1-9 SEM image of Si microsphere in diameter of 530 μm [19].
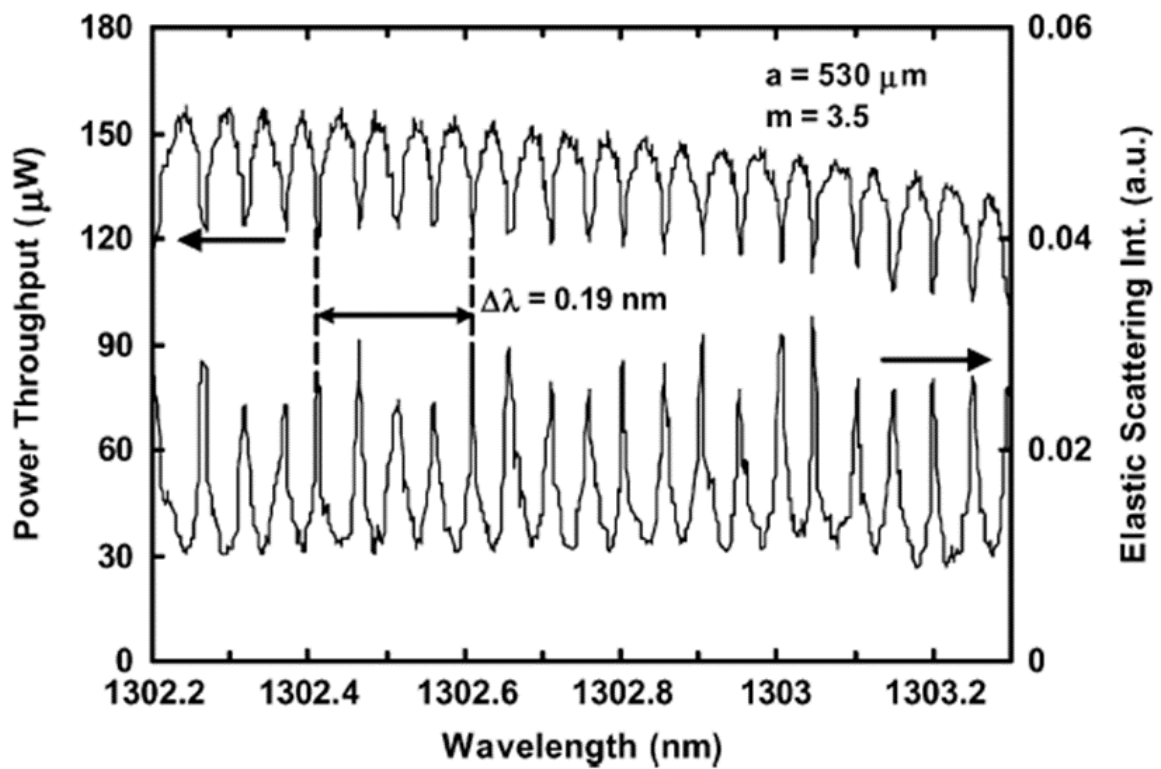
Fig. 1-10 Elastic scattering (bottom) and power transmission spectrum (top) from the Si microsphere [19].

1.3　Organization of the Thesis

In this thesis, the fabrication process of Si-cored fiber is described in details and high-Q WGMs Si microsphere resonators fabricated by using CO_2 laser reformation over a pure Si-core are reported in details as well. Chapter 1 describes the motivation of this thesis and reviews on up-to-date results about fabrication of Si-cored fibers and Si-based WGMs resonators reported by other groups including the fabrication, characteristics measurement. In Chapter 2, we proposed a homemade Si-cored fiber drawing system for fabricating Si-cored fibers and measurement of optical, material characteristics in Si-cored fibers. After fabrication of Si-cored fibers, the Si-cored tapered fibers fabricated by drawing twice will be demonstrated in Chapter 3. Chapter 4 shows the fabrication process of Si microsphere and the optical properties including WGMs resonance and thermo-optic effect. Chapter 5 is the conclusion of this thesis and future works will be mentioned.

Chapter 2   Fabrication of Si-cored fibers and Their

Optical, Material Characteristics
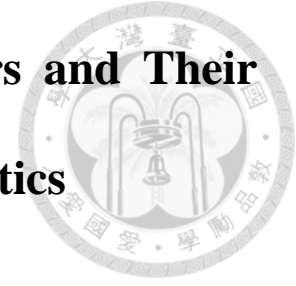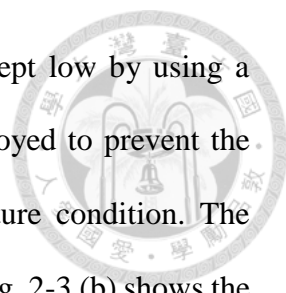
2.1   Fabrication of Silicon-Cored Fibers

2.1.1   Fabrication Process

With the information carrying capacity increasing, the conventional electrical circuits gradually become difficult to afford it. Therefore, more and more research about the Si photonics [1] emerging in the last decade. Due to the motivation from the Si photonics and fiber optics in silica materials [24], a novel concept about combination of semiconductor core and silica cladding was proposed in 2006 [2]. The first one demonstrated Si-cored fiber by using high pressure chemical vapor deposition technique, but it is time-consuming and impossible for high product throughput.

We adopted an alternative method to fabricate Si-cored fibers. The technique of powder-in-tube and vertical-drawing are combined by ourselves for fabricating Si-cored fibers. The polycrystalline Si powders (purity: 99.999%) have an average size of ca. 100 μm were packed into a fused silica tube whose outer and inner diameters were 10 mm and 2 mm, respectively. One end of the fused silica tube was sealed by using oxy-hydrogen flame as shown in Fig. 2-1. Then the powder-packed fused silica tube was drawn in a homemade drawing tower at some suitable temperature varying from 1600 to 1720 ℃. The homemade drawing tower mentioned before was fabricated by our own group, the heater inside was made of graphite whose melting point was around 3600 ℃. A front view of the homemade drawing tower is shown in Fig. 2-2. In this temperature range, the Si powders would melt and the fused silica tube would become softened.

During the drawing process the air pressure inside the tube was kept low by using a mechanical pump with nitrogen. These nitrogen pumped was employed to prevent the graphite heater from oxidation happened under the high temperature condition. The undesired oxidation on the graphite heater is shown in Fig. 2-3 (a). Fig. 2-3 (b) shows the graphite heater inside the furnace and two bronze electrodes. It was found that the drawing temperature would significantly affect the crystallinities and the morphologies of the Si core. At a temperature of 1580 $^{\circ}$C, the Si-cored fibers were easily broken during the drawing process. Since the melting temperature and softening point of fused silica were ca. 1732 $^{\circ}$C and 1630 $^{\circ}$C, respectively, the silica cladding would not become softened enough to sustain the force of drawing at 1580 $^{\circ}$C. Conversely, the Si-cored fibers could be continuously formed at 1720 $^{\circ}$C. With intensive study in the temperature-dependence of silica viscosity, the yield of Si-cored fibers in long length (over~1 m) were dramatically enhanced at 1650 $^{\circ}$C inside the furnace. Fig. 2-4 shows the preform in tapered shape with strong light emission just coming out from the furnace, and the tapered shape obviously indicated the silica cladding is softened enough to sustain the force drawing downward at 1650 $^{\circ}$C. With the appropriate temperature inside the furnace, the Si-cored fibers could be drawn at a high speed of 5~12 m/min with resultant silica cladding and Si core diameters being in the range of 100-300 μm and 10-30 μm, respectively. Three optical microscope pictures of drawn Si-cored fibers in different sizes are shown in Fig. 2-5 (a)-(c). Both (a) and (b) are the side views, (a) is Si core and silica cladding in the diameter of 11 and 109 μm; (b) is Si core and silica cladding in the diameter of 21 and 195 μm; (c) is the cross-section view of the same fiber in (b) after end being polished. The resultant Si-cored fibers with cladding diameter under ~300 μm could be bent like a curve. Fig. 2-6 (a) shows a Si-cored fiber is flexible enough to be coiled around a commercial fiber spool with 15 cm diameter. Moreover, a Si-cored fiber with smaller cladding diameter of

~200 μm could be bent to become a 2.5 mm radius circle to show its flexibility as shown in Fig. 2-6 (b). Besides the flexibility of the as-fabricated Si-cored fibers, for example, a 130 cm-long Si-cored fiber in our study as shown in Fig. 2-7. This method was able to fabricate meters long Si-cored fibers, this is also the reason why we adopt such method for making Si-cored fibers.
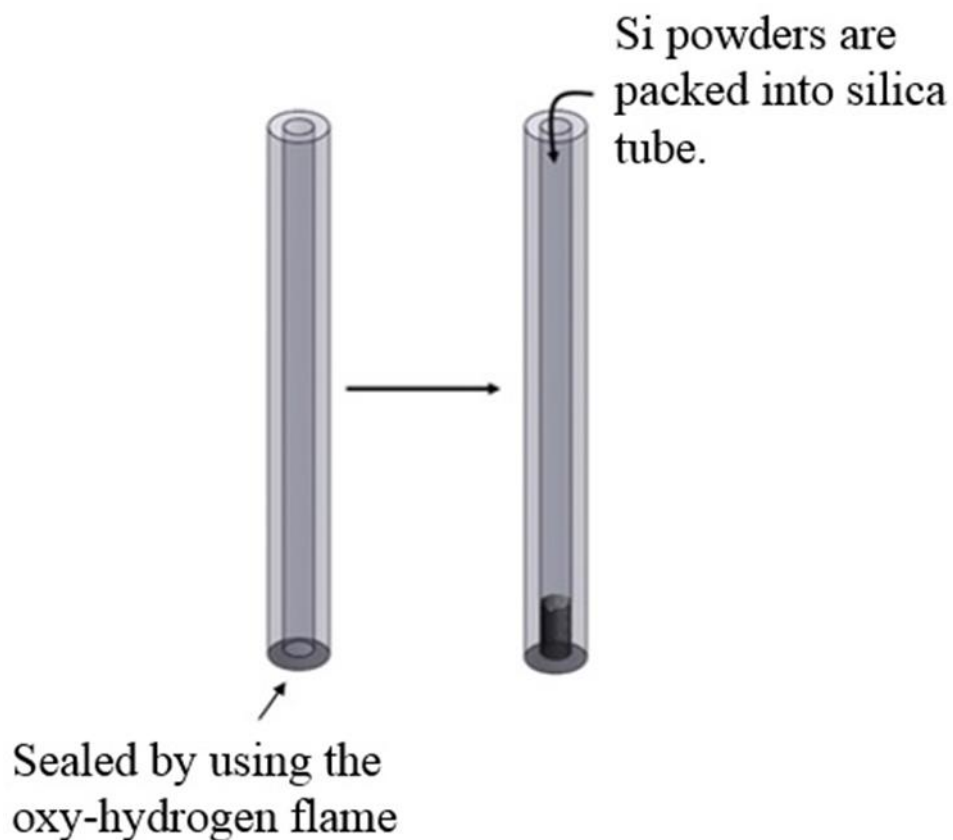
Fig. 2-1 Schematic diagram showing Si powders are packed into a silica tube.

Fig. 2-2 A front view of the homemade drawing tower.

(a)

(b)

Fig. 2-3 (a)The undesired oxidation happened on the surface of the graphite heater. (b)The

graphite heater inside the high temperature furnace and two bronze electrodes.

Fig. 2-4 A fiber preform in tapered shape with strong light emission just coming out from the furnace.
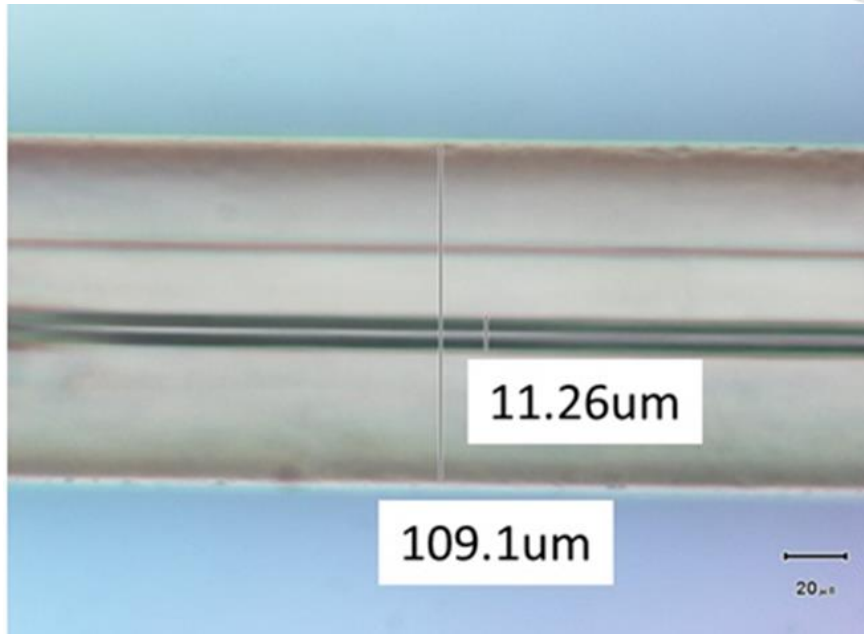
(a)
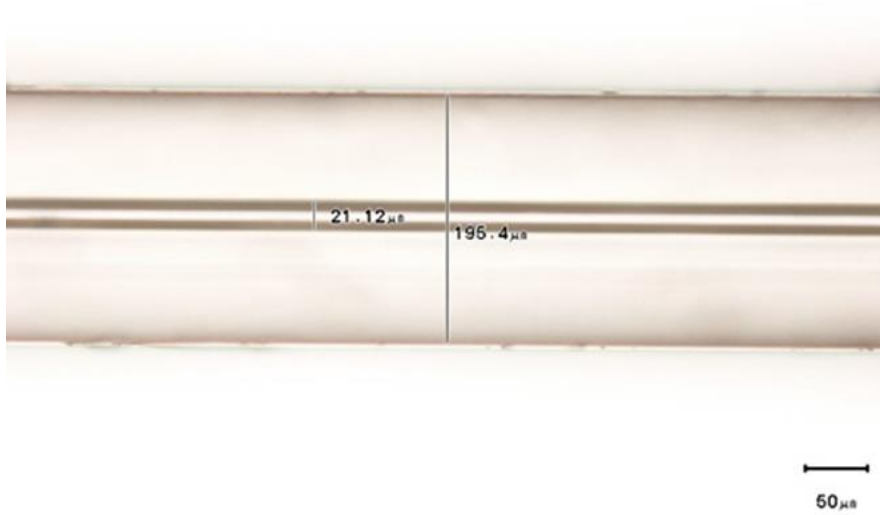
(b)

(c)

Fig. 2-5 (a) A Si-cored fiber with Si core and silica cladding in the diameter of 11 and 109 μm; (b) another Si-cored fiber with Si core and silica cladding in the diameter of 21 and 195 μm; (c) is the cross-section view.

(a)

(b)

Fig. 2-6 (a) Si-cored fibers in diameter under 300 μm could be coiled around a commercial

fiber spool in diameter of 15 cm. (b) a Si-cored fiber in diameter of 200 μm could be bent

to become a 2.5 mm radius circle to show its flexibility.
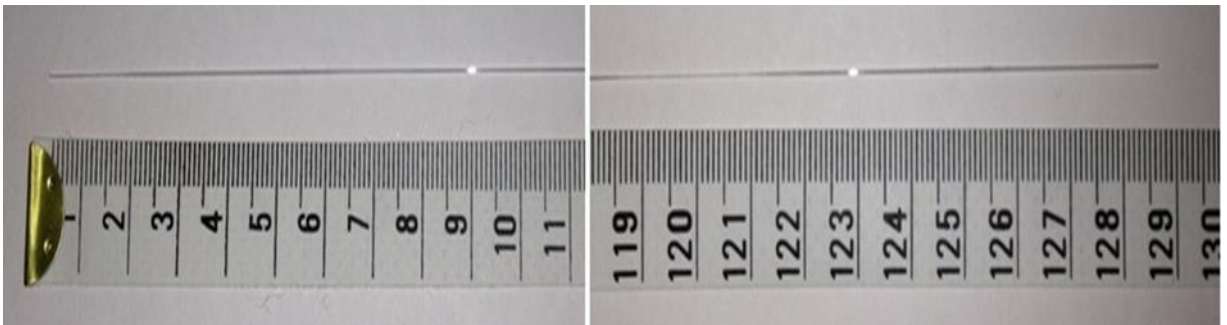
Fig. 2-7 A total 130 cm-long Si-cored fiber of our best work.

2.1.2 Element Analysis by Using Energy Dispersive Spectroscopy

Although we employed a nitrogen pump to prevent the interaction between oxygen in the air and molten Si, we still want to indeed understand real compositional elements in Si-cored fibers. Therefore, we used energy dispersive X-ray spectroscopy (EDS) to quantitatively determine the composition of Si and oxygen elements in core and cladding regions.

EDS, sometimes called energy dispersive X-ray analysis (EDXA) or energy dispersive X-ray microanalysis (EDXMA), is a common analytical technique used for the elemental analysis or chemical characterization of a sample. It relies on an interaction between some source of X-ray excitation and a sample, and the principle of EDS is shown in Fig. 2-8(a). Its characterization capabilities are due in large part to the fundamental principle that each element has a unique atomic structure allowing unique set of peaks on its X-ray emission spectrum. To stimulate the emission of characteristic X-rays from a specimen, a high-energy beam of charged particles such as electrons or protons, or a beam of X-rays, is focused on the sample being studied. At rest, an atom within the sample contains ground state (or unexcited) electrons in discrete energy levels or electron shells bound to the nucleus. The incident beam may excite an electron in an inner shell, ejecting it from the shell while creating an electron hole where the electron was. An electron from an outer, higher-energy shell then fills the hole, and the difference in energy between the higher energy shell and the lower energy shell may be released in the form of an X-ray. The number and energy of the X-rays emitted from a specimen can be measured by an energy-dispersive spectrometer. As the energy of the X-rays are characteristic of the difference in energy between the two shells, and of the atomic structure of the element from which they were emitted, this allows the elemental composition of the specimen to be measured [31].

27

A cross-sectional element distribution with a Si-cored fiber in core and cladding diameter of 85, 200 μm is shown in Fig. 2-8(b). And the result clearly indicates that the interface between the Si core and the silica cladding, and there are almost no oxygen atoms in the Si core except for the slight contamination.
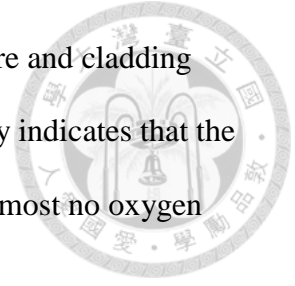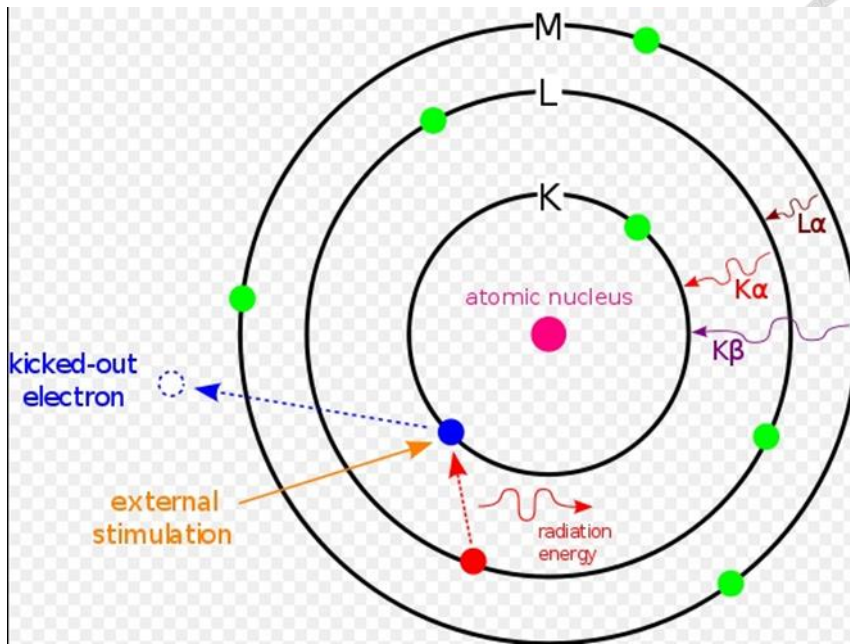
(a)
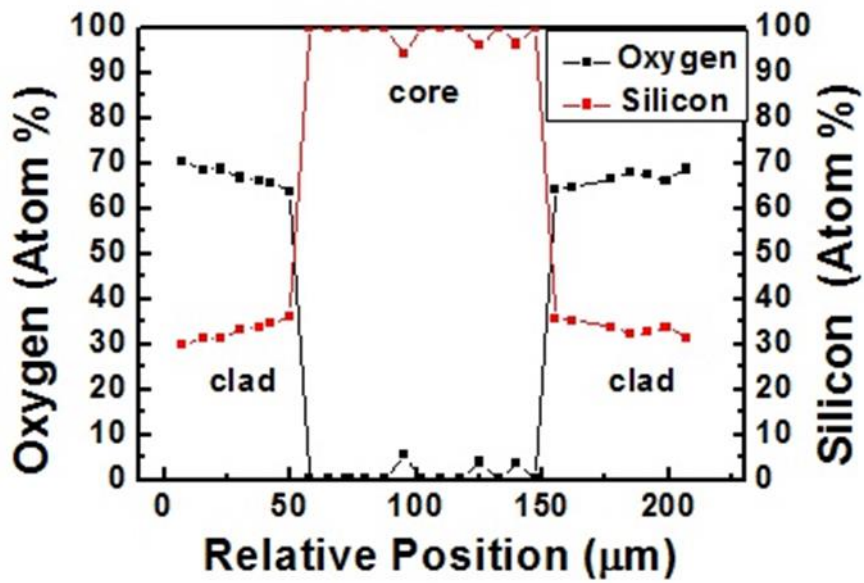
(b)

Fig. 2-8 (a) The principle illustration of EDS [31]. (b) The cross-sectional distributions of Si and O elements across a Si-cored fiber in core and cladding diameters of 85, 200 μm, respectively.
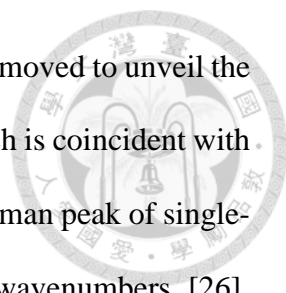
2.2 Material Characteristics of Silicon-Cored Fibers

2.2.1 Raman Scattering Spectrum

Raman spectroscopy is a spectroscopic technique used to observe vibrational, rotational and other low-frequency modes in a system [25]. It relies on inelastic scattering or Raman scattering of monochromatic light, usually from a laser in the visible, near infrared or near ultraviolet range. The laser light interacts with molecular vibrations, phonons or other excitations in the system, resulting in the energy of the laser photons being shifted up or down. The shift in energy gives information about the vibrational modes in the system. Typically, a sample is illuminated with a laser beam. Electromagnetic radiation from the illuminated spot is collected with a lens and sent through a monochromator. Elastic scattered radiation at the wavelength corresponding to the laser line (Rayleigh scattering) is filtered out, while the rest of the collected light is dispersed onto a detector by either a notch filter or a band pass filter.

Here, we measure the crystalline state of the Si-cored fiber by using Raman spectroscopy. Fig. 2-9(a) shows the Raman spectra of the single-crystal Si, Si-cored fibers in core diameter of 100 μm with or without silica cladding were measured using a commercial micro-Raman microscope (Protrustech, BWII) equipped with a monochromator having a focal length of 75 cm. The excitation laser in 532 nm wavelength was focused on the Si core through the transparent silica cladding when the Raman spectrum were taken. It's worth noting that the Raman shift happened after the silica cladding was removed in Fig. 2-9(a). The Raman peaks of the reference single-crystal Si wafer and the Si-cored fiber are located at 520.85 cm^{-1} and 519.5 cm^{-1}, respectively. It is apparent that the peak position (519.5 cm^{-1}) of the transverse optical (TO) mode of the Si-cored fiber is close to

that of single-crystal Si (520.85 cm^{-1}). After the silica cladding was removed to unveil the Si core, the TO mode shifted to the wavenumber of 520.85 cm^{-1}, which is coincident with that of the reference single-crystal Si. It has been reported that the Raman peak of single-crystal Si when subjected tensile stress would shift to shorter wavenumbers [26]. Therefore the amount of wavenumber short-shift, about 1.4 cm^{-1}, in the Si-core fiber indicates that the Si core is under a tensile stress. As shown in Fig. 2-9(b), the tensile stress in the Si core may originate from the difference of coefficient of thermal expansion (CTE) between silica and Si [26]. The CTEs of Si and fused silica are about 2.5 and 0.5 (10^{-6}/K), respectively [27, 28]. During the drawing process, the melting Si firstly conformed to the shape of the tube at 1650 ^{o}C, and then bonded to the fused silica tube when it began to solidify [29, 30]. Owing to the CTE difference, the Si being solidified would shrink more than that of the fused silica tube during cooling. Since the Si strongly adhered to its surrounding fused silica tube, the tube would exert a tensile stress to prevent the solidifying Si core from shrinking, therefore causing the Raman peak shifted to 519.5 cm^{-1}. After the silica cladding was removed from the Si-cored fiber, the tensile stress in the Si core was then released and the Raman peak returned to the one identical to the single-crystal Si wafer's (520.85 cm^{-1}). In order to investigate the uniformity of crystalline state of Si-cored fiber, a series of Raman spectrum were measured over 40 cm long at an interval of 2 cm, the results are shown in Fig. 2-10. The red curve measured from a single-crystal Si wafer is used as reference and the black curves are the Raman spectrum taken every 2 cm intervals, showing the same peak position (519 cm^{-1}) and almost the same bandwidth. This result indicates that the crystallinity of the Si core was uniform throughout the fiber.
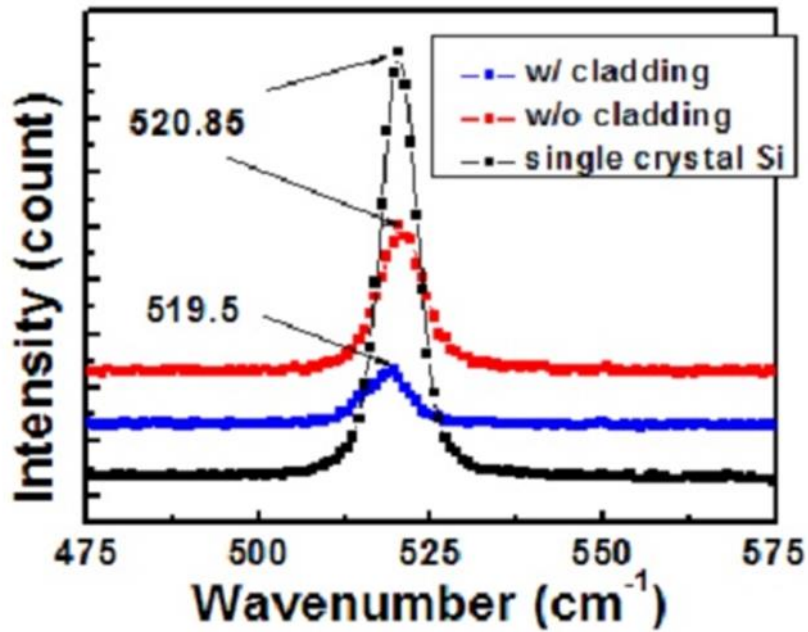
(a)
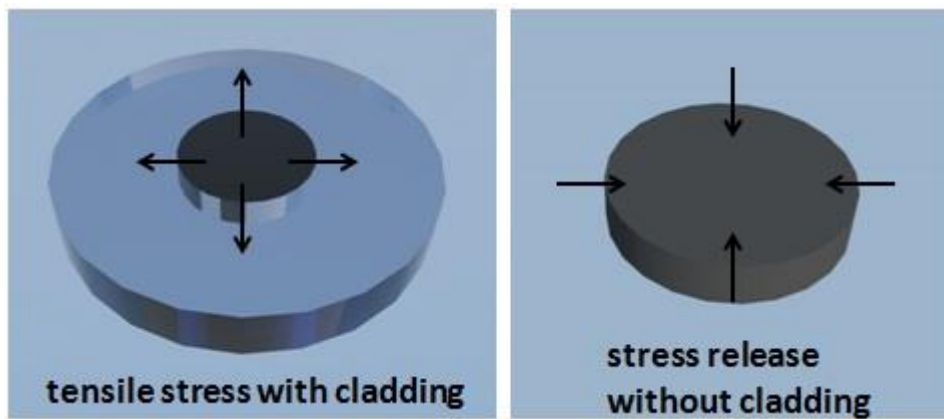
(b)

Fig. 2-9 (a) Micro-Raman spectra of reference single-crystal Si, Si-cored fibers with and without silica cladding. (b) A schematic illustration shows the tensile stress being exerted on a solidifying Si core caused by the CTE differences between silica and Si core, and the release of such stress when the silica cladding is being removed.
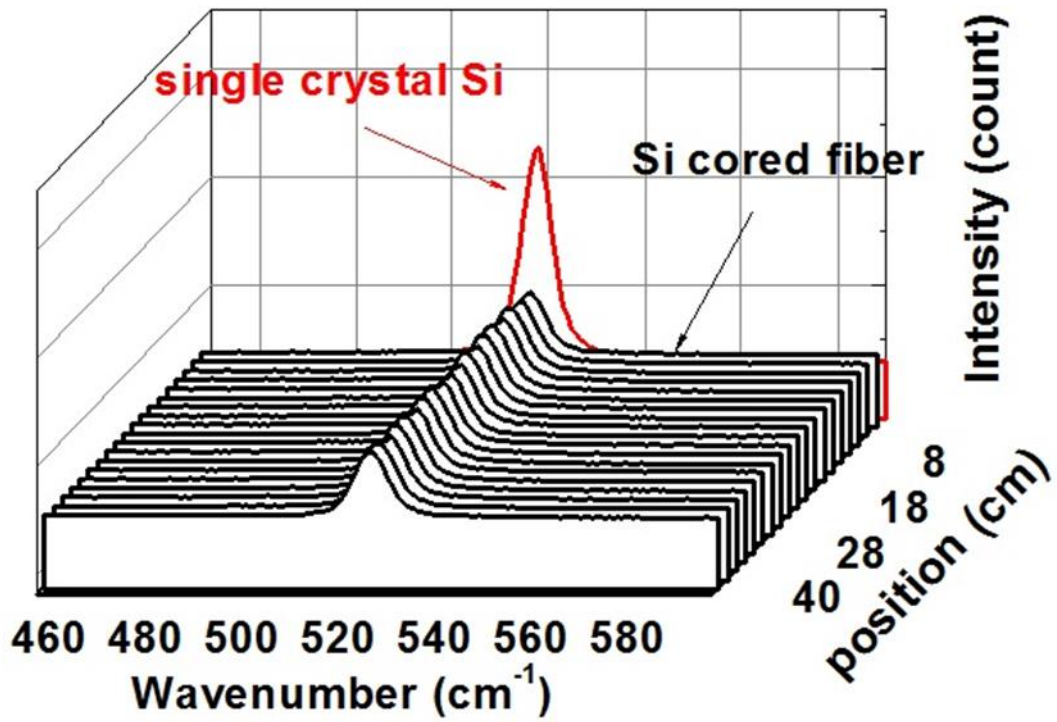
Fig. 2-10 The Raman spectra measured at an interval of 2 cm over its 40 cm length where

the reference spectrum in red is of single-crystal Si wafer.

2.2.2 High-Resolution Transmission Electron Microscope Image

High-resolution transmission electron microscopy (HRTEM) is an imaging mode of the transmission electron microscope (TEM) that allows for direct imaging of the atomic structure of the sample. HRTEM is a powerful tool to study properties of materials on the atomic scale, such as semiconductors, metals, nanoparticles and sp^2-bonded carbon.

A Si-cored fiber was sectioned by using a focused ion beam and its cross-section was examined by using HR-TEM (JEOL) operated at 200 keV. As shown in Fig. 2-11(a), uniform and periodical crystal lattices are clearly seen. No obvious defects such as dislocations, vacancies or grain boundaries were found, indicating that the defect free Si core was indeed of single-crystal phase. The calculated lattice plane spacing is 0.192 nm. The diffraction pattern from the selected sample area showed a 6-fold symmetry pattern, which is typically observed in the [110] Si (Fig. 2-11(b)). The results from the HR-TEM characterization are consistent with those of the Raman spectroscopy, both indicating that the Si core forms a single-crystal structure after optimizing the fabrication parameters.
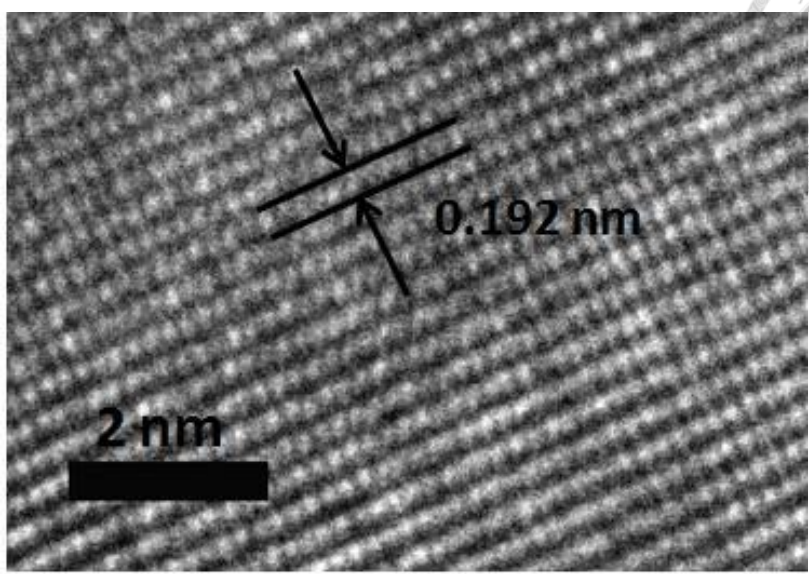
(a)
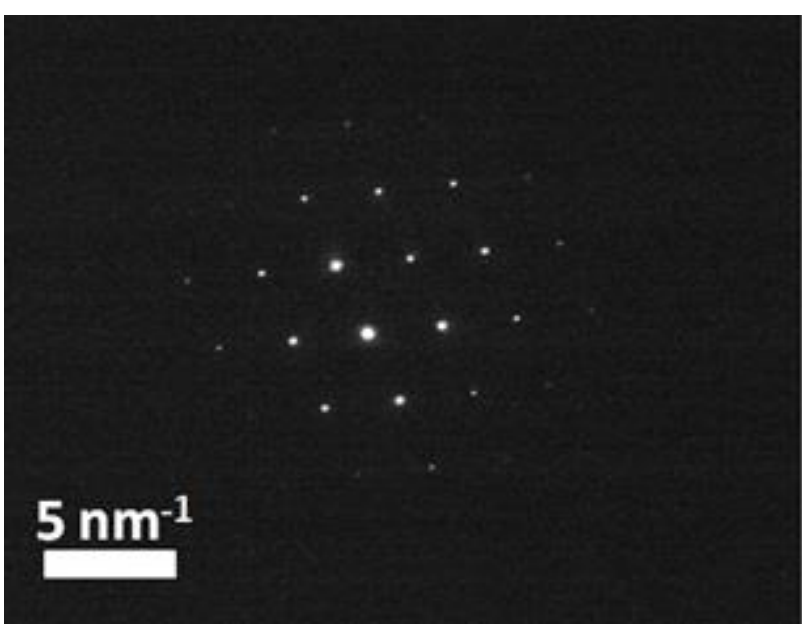
(b)

Fig. 2-11 (a) HR-TEM image of the cross-sectional area of a single-crystal Si-cored fiber.

(b) Diffraction pattern of [110] Si core.

2.3   Optical Characteristics of Silicon-Cored Fibers
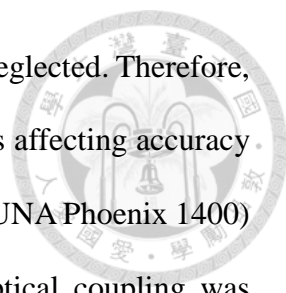
In addition to fabrication process and material analysis, the most important property is optical transmission loss owing to its fiber structure. Here, we measured the transmission loss of the Si-cored fibers by using the standard cut-back method. In telecommunications, a cut-back method is a destructive technique for determining certain optical fiber transmission characteristics, such as attenuation and bandwidth. The measurement technique consists of performing the desired measurements on a long length of the fiber under test, cutting the fiber under test at a point near the launching end, repeating the measurements on the short length of fiber, and subtracting the results obtained on the short length to determine the results for the residual long length. The transmission loss can be quantitatively expressed as a total attenuation α between two arbitrary points X and Y on the same fiber is

$$\alpha(\text{dB}) = 10 * \log_{10}\left(\frac{P_x}{P_y}\right)$$

Px is the power output at point X. Py is the power output at point Y. Point X is assumed to be closer to the optical source than point Y.   The attenuation coefficient or attenuation rate α is given by α(dB/km) = A/L. Here L is the distance between points X and Y. The benefit of this technique is that it allows measurement of the fiber characteristics without introducing errors due to variation in the launch conditions. For example, the coupling efficiency of the light source is kept consistent between the initial and the cutback measurements.

Notable some common contributors for transmission loss may be cracks, grain boundaries (poly-crystallinity), surface roughness, longitudinal perturbations, and impurity [32]. The cut-back method was adopted for the measurement in the wavelength ranging from 1520-1560 nm, and the experiment setup is shown in Fig. 2-12. In this

method, the factor of coupling loss between light source and fiber is neglected. Therefore, accuracies of the length and launching condition are the main factors affecting accuracy of the measurement [33]. Light was launched from a tunable laser (LUNA Phoenix 1400) through a lead-in single-mode fiber into a Si-cored fiber. The optical coupling was monitored by using a charge-coupled device to ensure that the light was properly delivered to the Si-cored fiber. The transmitted light was then collected by a power meter. As shown in Fig. 2-13(a) and (b), the measured transmission losses with a Si-cored fiber (core/cladding diameter: 130/813 μm) is ~0.3 to 0.4 dB/cm and another Si-cored fiber with smaller diameter (core/cladding diameter: 22.5/209 μm) is ~0.6 to 0.9 dB/cm in the wavelength regime from 1520 to 1560 nm. The error bar is resulted from the flatness on the end face of fiber during the cut-back process and can be further improved. Besides, we listed and summarized other group fabricating Si-cored fiber with different method all over the world in Table. 1. It is worth noting that the measured transmission loss of Si-cored fiber in our work is the smallest loss after the comparison with other groups' results.
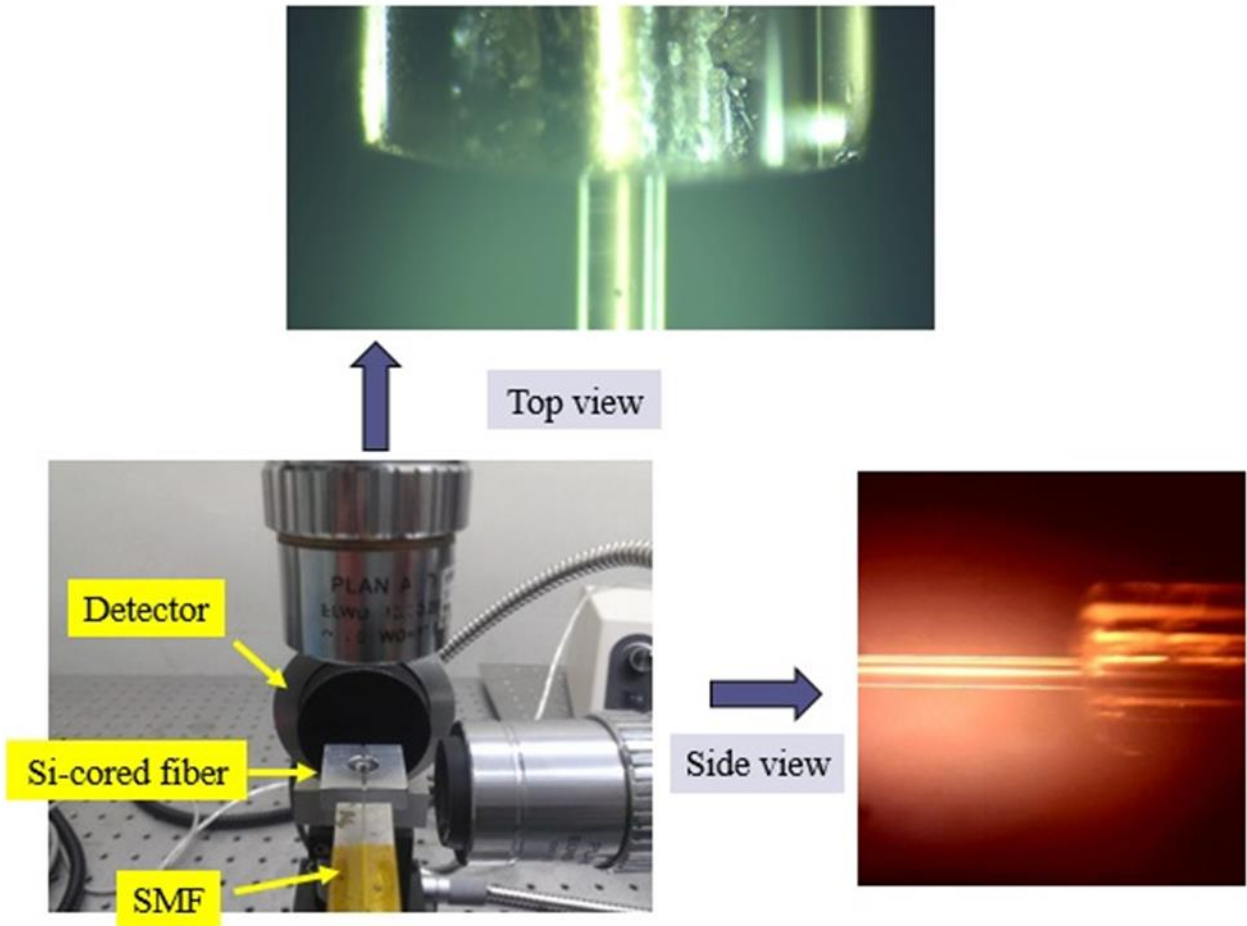
Fig. 2-12 The experiment setup of transmission loss measurement. SMF is the commercial single-mode fiber. Two cameras were used to real-time monitor the coupling condition in side, top view between a SMF and a Si-cored fiber. A photodetector was used to collect the transmitted light.
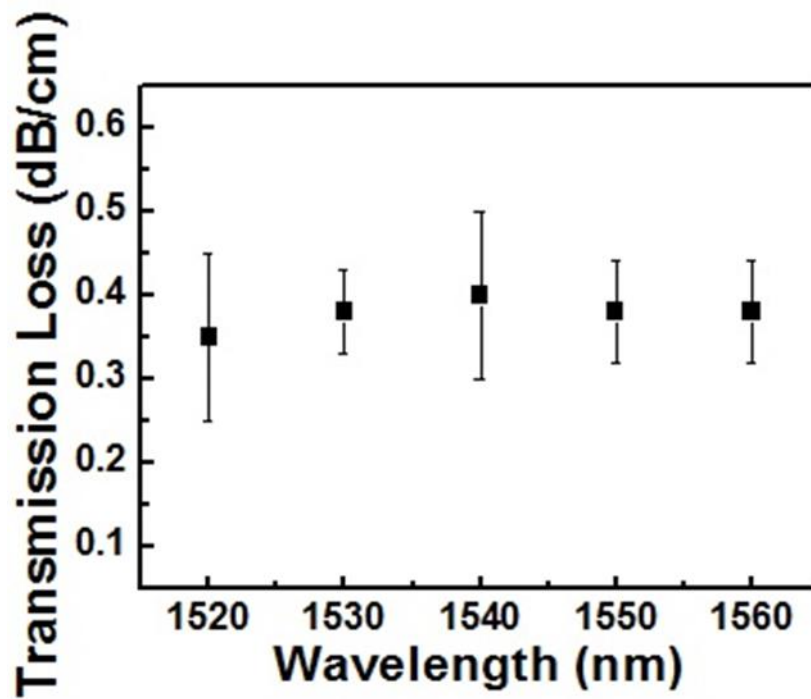
(a)
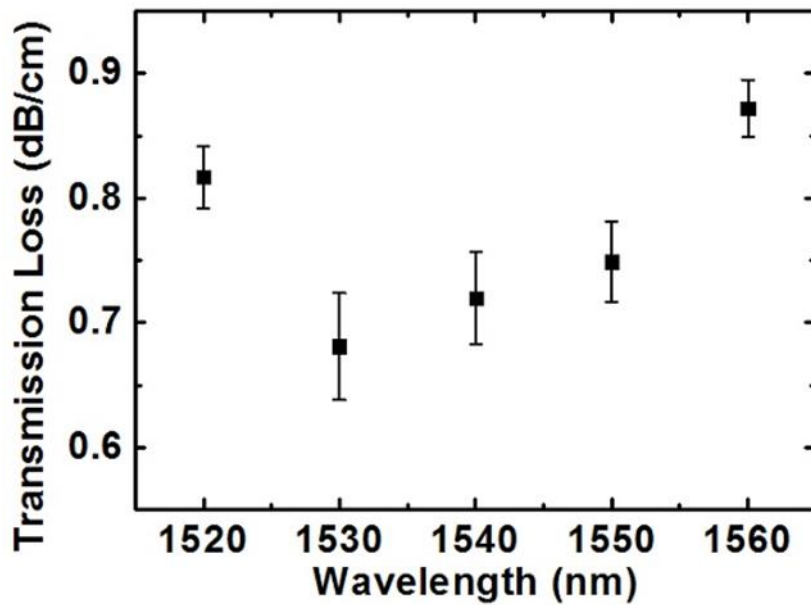
(b)

Fig. 2-13 (a) The measured transmission losses of a Si-cored fiber (core/cladding diameter:

130/813 μm) and (b) is another Si-cored fiber with smaller size (core/cladding diameter:

22.5/209 μm) ranging from 1520 to 1560 nm.

Source material	Fabrication method	Crystalline State	Transmission Loss(dB/cm) in measured wavelength	Core diameter (μm)	Reference
Precusors for a-Si:H	HPCVD	Amorphous	2.5 at 1.55μm	5.6	[34]
Precusors for a-Si:H	HPCVD	Poly-crystalline	8 at 1.55μm	6	[35]
Single-crystal Si rod	Molten core drawing	Highly-crystalline	0.043 at 2.936μm	50	[21]
Single-crystal Si powders	Molten core drawing	Highly-crystalline	9.7 at 1.3μm	200	[32]
Poly-crystalline Si powder	**Molten core drawing**	**Single-crystalline**	**0.3-0.9 at 1.55μm**	**20-200**	**This work**

Table. 1 Comparison between the reported Si-cored fibers and this work in terms of source materials, fabrication methods, crystallinity of fiber cores, transmission losses and core diameters.

2.4　Summary

In this chapter, Si-cored fibers are introduced. We demonstrate that single-crystal Si-cored fibers can be obtained by using a rapidly vertical drawing method. The use of low-cost polycrystalline Si powders as the preform material is an economic way of fabricating high quality meter-long single-crystal Si-cored fiber. By optimizing the processing temperature at around 1650 ℃, the soften silica cladding could still provide substantial confinement on the molten Si core during the drawing process. At the drawing speed of ca. 10 m/min, the rapid and dramatic reduction in the cross-sectional area generates a strong stress and spatial confinement on the Si core, making single crystalline possible. The crystallinity transformation from polycrystalline powders into single-crystal phase has been investigated and confirmed by using both the micro-Raman spectroscopy and HR-TEM. According to the HR-TEM images and micro-Raman spectra, the Si core possesses outstanding properties, including single crystallinity, high purity and high uniformity throughout the meters long fiber. The transmission losses is approximately 0.3 to 0.9 dB/cm of the Si-cored fibers in the optical communication regime are much lower than those reported previously.
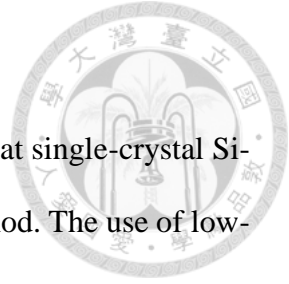
Chapter 3 Fabrication and Optical Characteristics of Silicon-Cored Tapered Fibers

3.1 Introduction to Silicon-Cored Tapered Fibers

With the size of modern electronics and photonics devices shrinking, the importance of micro- and nano-scale waveguides is gradually enhanced. Micro- and nano-scale waveguides have played an integral role in the recent success of Si photonics forming the basis of a number of compact optoelectronic devices [36]. In addition to possibility of integration, these micro- and nano-scale waveguides can also directly be used as a spot-size converter to connect with other Si photonics devices [37]. Due to the relationship between the optical nonlinearity and cross-section area of waveguide, the waveguide with smaller dimension can extremely enhance the nonlinearities, such as Kerr effect [38], especially for these materials with high refractive index, like Si, chalcogenide glass and so on. The number of guided modes is also mainly dependent on the size of waveguide, it is an effective method for decreasing the numbers of guided modes by shrinking the size of waveguide. Moreover, the simulated calculations in the number of guided modes with different dimension of Si-cored fiber are shown as follows. Some researches regarding to Si tapered waveguide have been reported. A three-dimensional Si taper have been fabricated by using a glass mask with ultraviolet lithography, dry etching on a silicon-on-insulator substrate, whose process details are shown in Fig. 3-1 [39]. Another report on tapered Si optical fiber have been made in 2008, in which a Si-cored fiber was tapered by using a fusion splicer. Smaller starting core diameters around 5.6μm, 2.7μm and 1.3μm were demonstrated. Due to the short moving range of the fusion splicer, so the tapering length was barely 700μm. The smallest core diameter is 500nm with starting

diameter of 1.3μm, and the cross-section view of microscope image is shown in Fig. 3-2. However, it is a little regretful that no measurement of transmission loss is shown in this paper [36].

In order to extend the potential applications of Si-cored fibers, we try to reduce the dimension of the Si-cored fiber by using a similar drawing method presented previously in our group for fabricating the silica microfiber [40].

Step 1 : spin coat photoresist
SOI
← photoresist

Step 2 : UV exposure using HEBS grayscale mask
SOI
← grayscale mask

Step 3 : develop
SOI
← photoresist

Step 4 : etch
← silicon

input coupler   central waveguide   output coupler
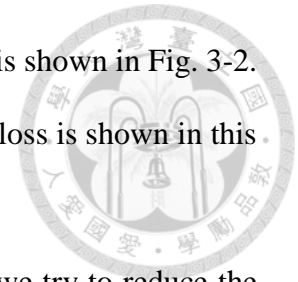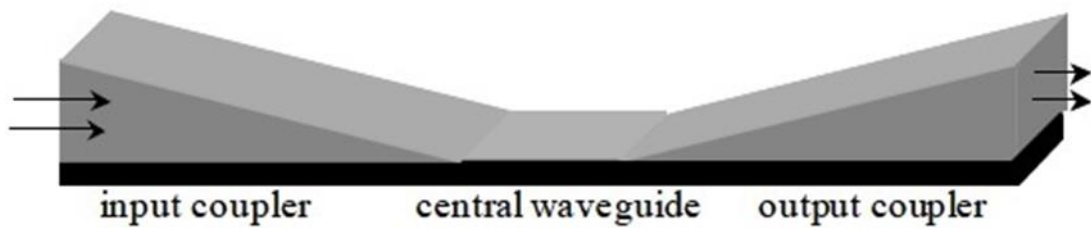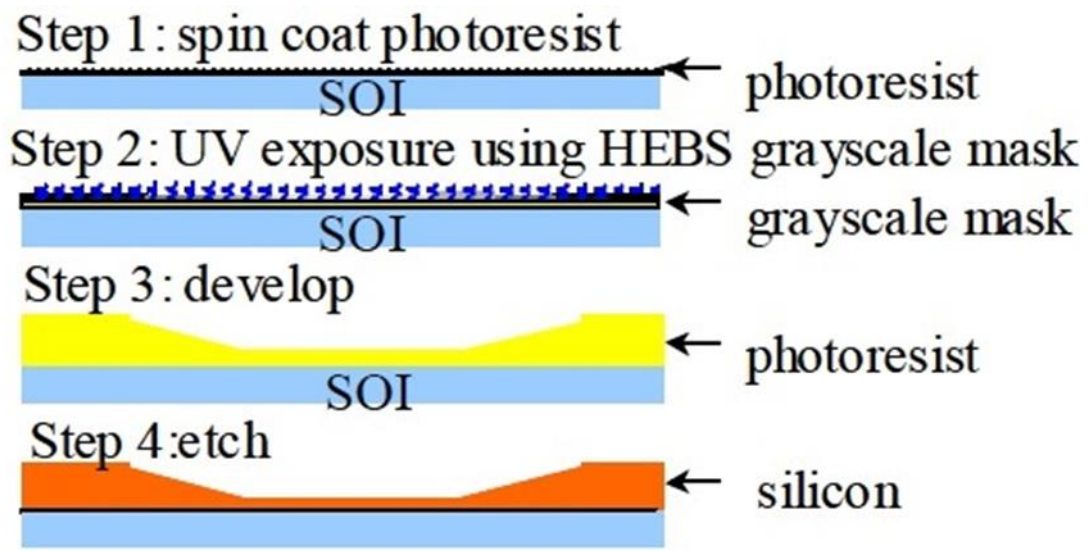
Fig. 3-1 (Top)The schematic of the fabrication process for 3-dimensional Si taper structure. (Bottom)The schematic of the propagation direction of input and output light [39].
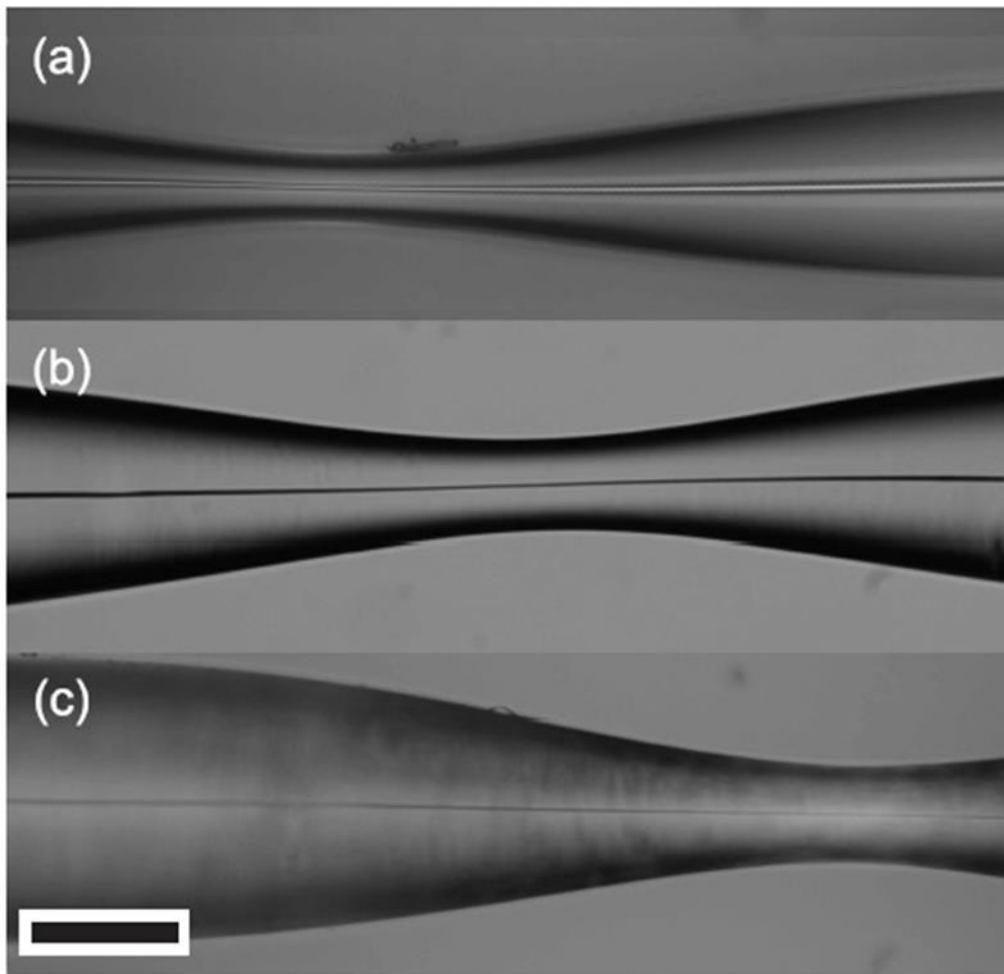
Fig. 3-2 Microscope images of the longitudinal taper profiles for starting fiber core diameters of (a) 5.6μm, (b) 2.7μm, and (c) 1.3μm. The 70μm scale bar is applicable for all images [36].

3.2   Fabrication of Silicon-Cored Tapered Fibers

3.2.1   Setup of Miniaturized Fiber Drawing Tower

Fiber drawing tower is the equipment which makes the optical fiber [41-43]. The whole system includes a furnace, a drawing mechanism, a coating and curing process, a diameter measuring and feedback control, and finally an optical fiber take-up machine. All these subsystems have to be integrated with parameters settled carefully and then the optical fiber can be manufactured in ultra-long length without broken. The temperature of the furnace, for instance, should be controlled in order to preserve a stable neck-down shape [44]. The gas flow was purged into the furnace to minimize the defect, which can also adjust the temperature profile and the viscosity of glass [45]. After leaving the furnace, the fiber was cooled before coating to prevent meniscus effect and formation of bubble. The coating machine should be pressurized to fit the requirement of high speed drawing [46]. The diameter and tension of optical fiber can be measured in situ and feedback to control the stability of fiber drawing [47, 48].

A microfiber have be made by drawing an optical fiber preform down to a microfiber in a diameter of few micrometers in our previous work. In the past work for making silica microfiber, the preform used in the experiment was a single-mode optical fiber in core/cladding diameter of 8.2μm/125μm [49]. The fiber preform with both ends being fastened to a fiber feeder and a drawing wheel respectively passed through a hot zone where the silica material became viscous liquid. Both the feeder and the wheel moved in the same direction at different speeds but with the desired constant ratio. By controlling the feed velocity (V_f) into the hot zone to be much slower than the drawing velocity (V_d), the fiber perform would be narrowed down based on the principle of mass conservation;

therefore, the resultant diameter reduction D_f/D_d can be related to the speed ratio

V_d/V_f as
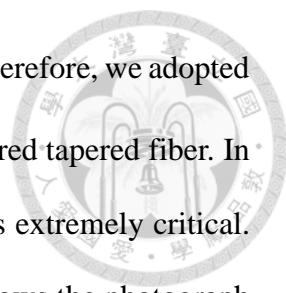
$$V_f \times D_f^2 = V_d \times D_d^2 \qquad (2.1)$$

where D_f and D_d are the diameters of fiber preform and MNOW, respectively.

Here we propose a modified miniature fiber drawing tower (MMFDT).The MMFDT is a small version of a traditional fiber drawing tower. The MMFDT comprises only a heat source, drawing mechanisms and several sets of regulators. The other subsystems such as feeding mechanisms and diameter measurement are neglected. Fig. 3-3 shows the experimental setup of MMFDT. The whole system was below 50 cm in height. We adapted the hydrogen oxygen flame to produce a Si-cored tapered fiber whose diameter smoothly varied from a few hundreds of μm to several μm. The highest temperature of hydrogen oxygen flame could reach up to 3000 ℃, which was sufficient to soften the silica cladding and further beyond the melting temperature of Si (1414 ℃) to make Si liquefied. However, an accompanying problem was caused by the fact that the fiber preform was heated from the lateral side and the tapered fiber would be readily bent if the tensile strength was not balanced at both ends. Hence we need to control the hydrogen oxygen flame, drawing stage simultaneously to prevent the flame contacting the microfibers after the drawing stops.

Some parameters have to be taken care to further improve the yield of tapered fiber drawing including the distance between the flame and the fiber preform, the speed of drawing, and the gas flow rate of hydrogen oxygen flame. The hydrogen oxygen flame could be divided into light blue inner cone and colorless outer cone. The temperature of inner cone was as high as 3000 ˚C, and the temperature of colorless outer cone was over
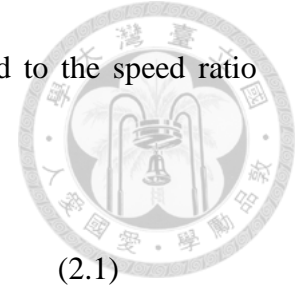
1400 ℃, which was insufficient to liquefy Si core inside cladding. Therefore, we adopted the light blue inner cone of hydrogen oxygen flame to drawing Si-cored tapered fiber. In addition, the control of gas flow rate of hydrogen oxygen flame was extremely critical. We controlled the gas flow rate by two sets of regulators. Fig. 3-4 shows the photograph of two sets of regulators whose flow rates were 2500 c.c / min and 100 c.c / min, respectively. The right one with flow rate 100 c.c / min was used for fiber drawing, and the left one, 2500c.c/min, was used for gas releasing. During the drawing process, we set the gas flow rate at the level of 70 c.c / min. At this level, the shape of flame was similar to a sphere, which made the flame stable enough for smooth fiber drawing.

The drawing speeds not only decided the diameter of microfibers but also determined the success of drawing conditions. If too slow for the drawing speed, the tapered fiber would be bent in the waist section or the not continuous Si core happened. Such bending in the waist section could induce a large optical loss for transmission. Besides, if the heat of flame was not high enough to soften the silica cladding instantly, such a high drag force would break the fiber preform.
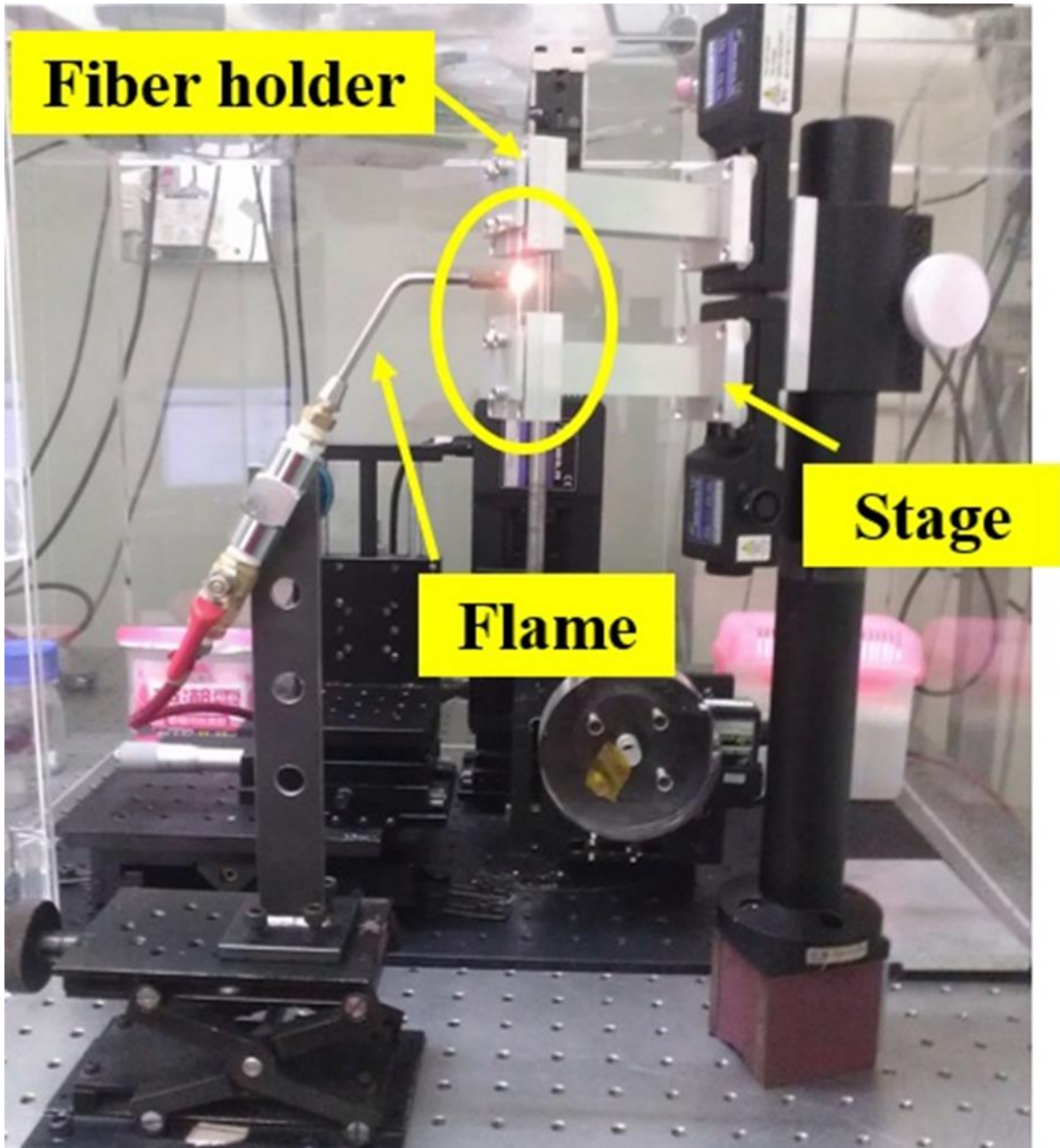
Fig. 3-3 The experimental setup of modified miniature fiber drawing tower.
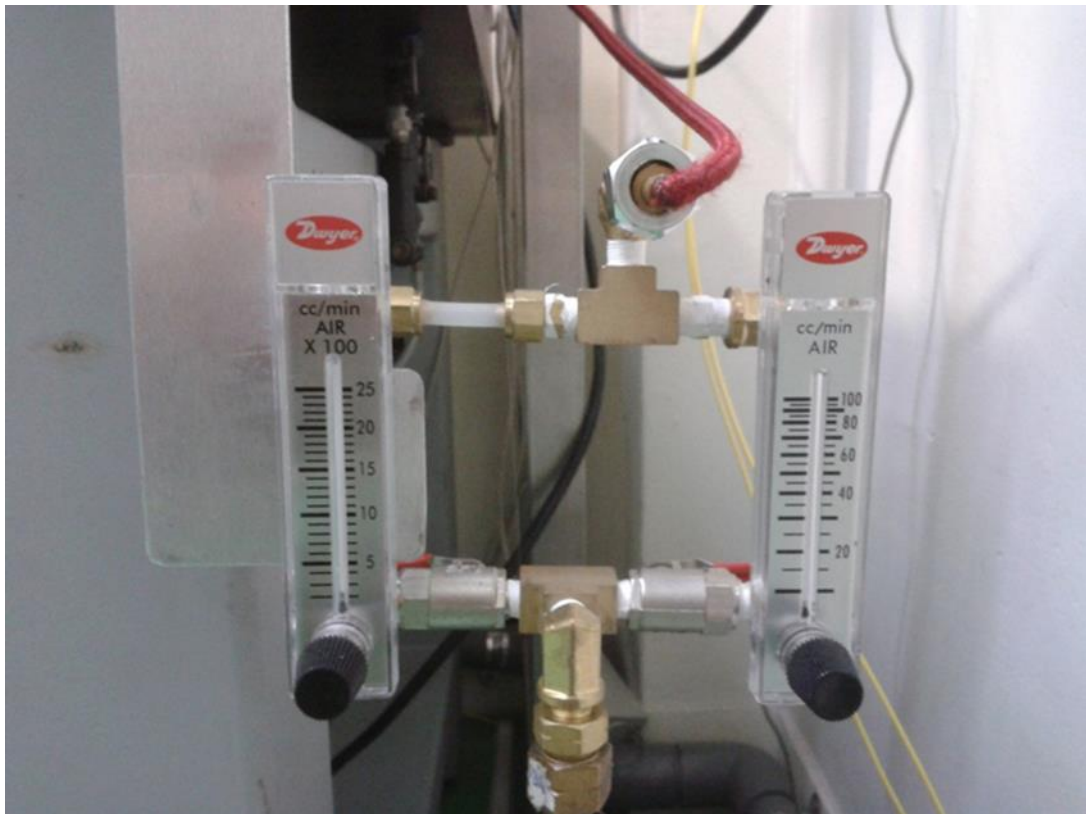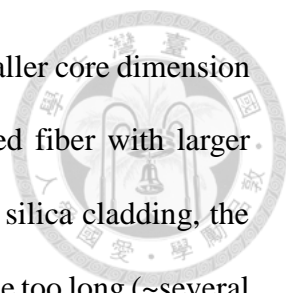
Fig. 3–4 Two regulators used to control the gas flow rates of hydrogen oxygen flame.

3.2.2 Fabrication Process of Silicon-Cored Tapered Fibers

To demonstrate the potential of Si-cored tapered fiber, we taper the Si-cored fiber mentioned before by using a hydrogen oxygen flame as heat source and the modified minimized fiber drawing tower. We choose Si-cored fibers in the diameter of cladding/core ranging from 300/30 μm to 100/10 μm for tapering. Before the tapering, we have to cleave the both end-facets of Si-cored fiber by using a fiber cleaver for silica single mode fiber in order to couple light into Si-cored tapered fiber. After a Si-cored fiber was fixed on the stage, check the gas flow be stable, make sure the flame shape like a sphere, then tapering can be started.

A Si-cored fiber fixed on the transition stage was moved into the center flame region, after a few seconds for heating, the Si core region would emitted extremely strong white light indicating the quite high temperature and the solid Si have transformed into the liquefy Si. The strong emission picture is shown in Fig. 3-5. When the Si-cored fiber emitted strong white light, the transition stage was moving downward for tapering the Si-cored fiber into tapered fiber. We had to instantly move the transition stage when the white light from Si-core emitted. Otherwise, the Si-cored fiber would be twisted due to the liquefy Si core could not provide a force to support the original shape. A Si-cored fiber in an original core/cladding diameter of 20/115 μm was chosen for making Si-cored tapered fiber. The 20 μm core diameter was tapered to 2.6 μm, and 115 μm cladding diameter was tapered to 13 μm in the waist section as shown in Fig. 3-6(a). Fig. 3-6(b) shows a series of microscope images of a Si-cored tapered fiber from one end to the other end. The total taper-to-taper distance is ~ 2 cm, which is determined by the moving distance of the transition stage. Such tapering length is far beyond the previously reported by using a fusion splicer to tapering in 2010 [36]. These images show that the tapering process has produced a continuous, defect free, Si core with a smooth transition from the

51

untapered fiber to the taper waist. In addition to tapering with this smaller core dimension (core diameter ~ 20 μm), we also tried to fabricate Si-cored tapered fiber with larger dimension. Due to the larger several times in volume of Si core and silica cladding, the heating time for making solid Si core transformed into liquid Si became too long (~several minutes). Such too long heating time increased the difficulty for tapering, part of Si core liquefied earlier would flow and soften silica cladding would be twisted in order to fail in tapering. A Si-cored tapered fiber in a starting core diameter of 65 μm have been successfully demonstrated, the core diameter was tapered to 29 μm, as shown in Fig. 3-7. The tapering length was shorter, only ~ 2 mm.
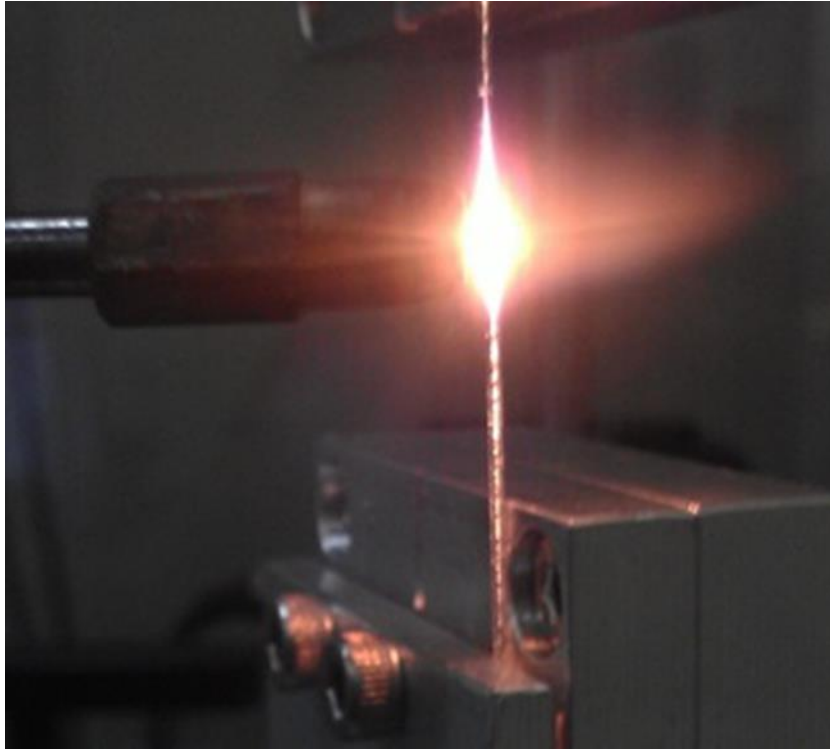
Fig. 3-5 A Si-cored fiber was fixed on the transition stage. When the Si core region emitted extremely strong white light, it indicated that the quite high temperature was reached and the solid Si was transformed into the liquefy Si.
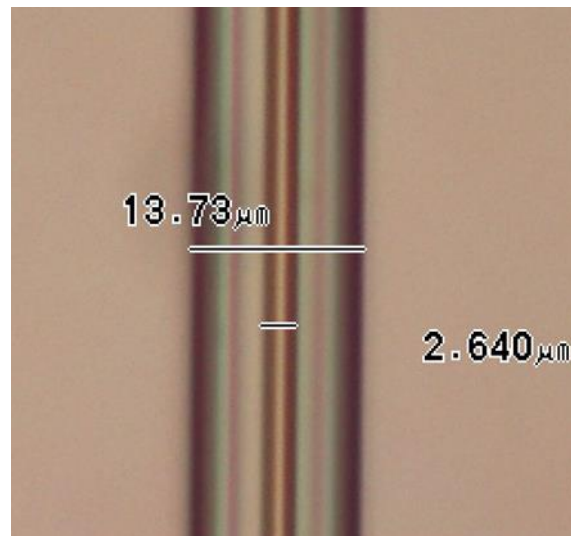
(a)

(b)

Fig. 3-6(a) A Si-cored tapered fiber with core diameter of 2.6 μm in the waist section. (b)

A series of microscope images show that a resultant Si-cored tapered fiber with the total

taper-to-taper length is ~ 2 cm.
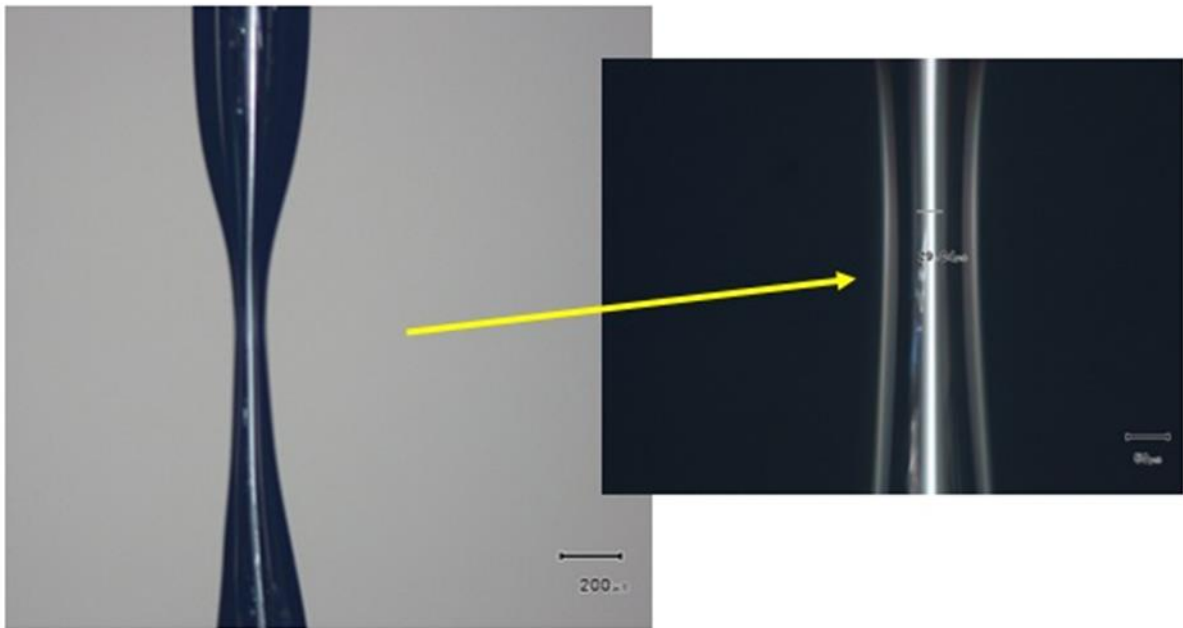
Fig. 3-7 A Si-cored tapered fiber with a larger starting core diameter of 65μm, which was tapered to 29 μm finally.

3.3 Optical Characteristics of Silicon-Cored Tapered Fibers

3.3.1 The Number of Guided Modes

Due to the small dimension of Si-cored tapered fiber, the number of modes would be reduced when compared with the original Si-cored fiber. Here we used the three-layer model in MATLAB [50] to simulate the effective indices of different modes in the Si-cored tapered fiber. The three-layer model, as implied by the name, includes the core, cladding, and surrounding layers for the simulation. The two boundaries between the layers were simultaneously solved and the tangential and axial electric fields (eϕ, ez) and magnetic fields (hϕ, hz) should be continuous. The effective indices thus solved in different diameters at the wavelength of 1550 nm are shown in Fig. 3-8. The blue, green, red, yellow, cyan and magenta lines represent HE1m, HE2m, HE3m, HE4m, TE and TM modes, respectively. There are several modes (~220) at 20 μm core diameter of Si-cored fiber. The diameter of Si-cored tapered fiber satisfying single-mode operation criterion lies in 377 nm [51], and the simulation result is also shown in Fig. 3-8. It is observed that the effective indices are far from the refractive index of Si core of 3.48 and silica cladding of 1.45, implying that these modes were mostly guided in core region and large index difference of Si and silica induced the strong guiding mechanism.

The number of guided modes in Si-core was dramatically reduced to 36 after tapering the Si-core from 20 to 2.6 μm in diameter as shown in Fig. 3-9. Such simulation results clearly show that this tapering process can effectively provide a function for reducing the guided mode in a fiber device.

56

The number of modes: 220 @Si core=20μm
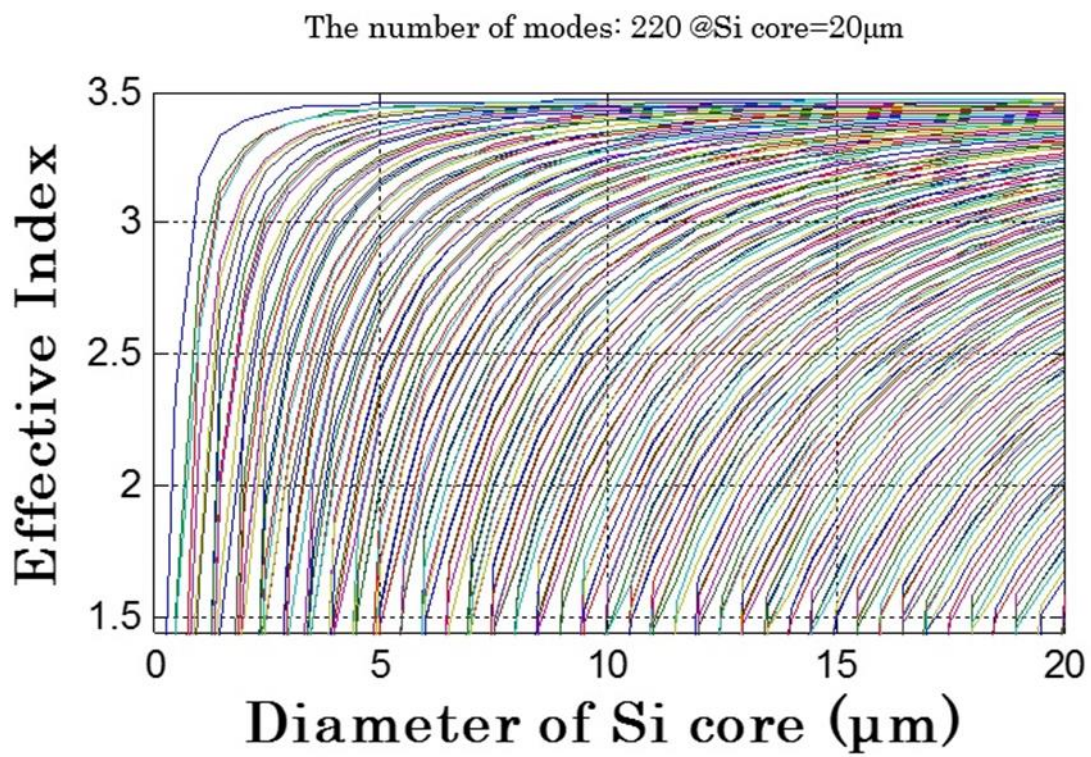
Fig. 3-8   The effective indices of different modes of Si-cored tapered fiber smaller than

20 μm in diameter at the wavelength of 1550 nm.
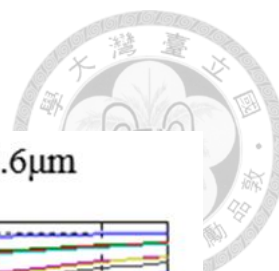
The number of modes: 36 @Si core=2.6μm
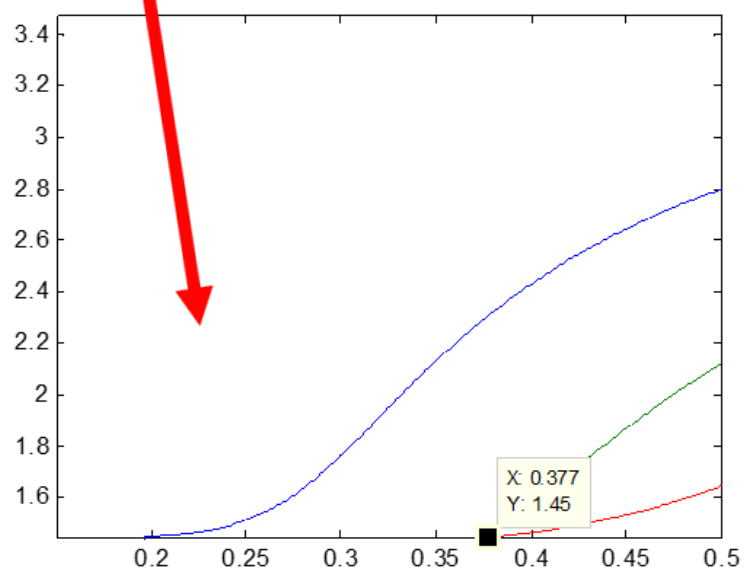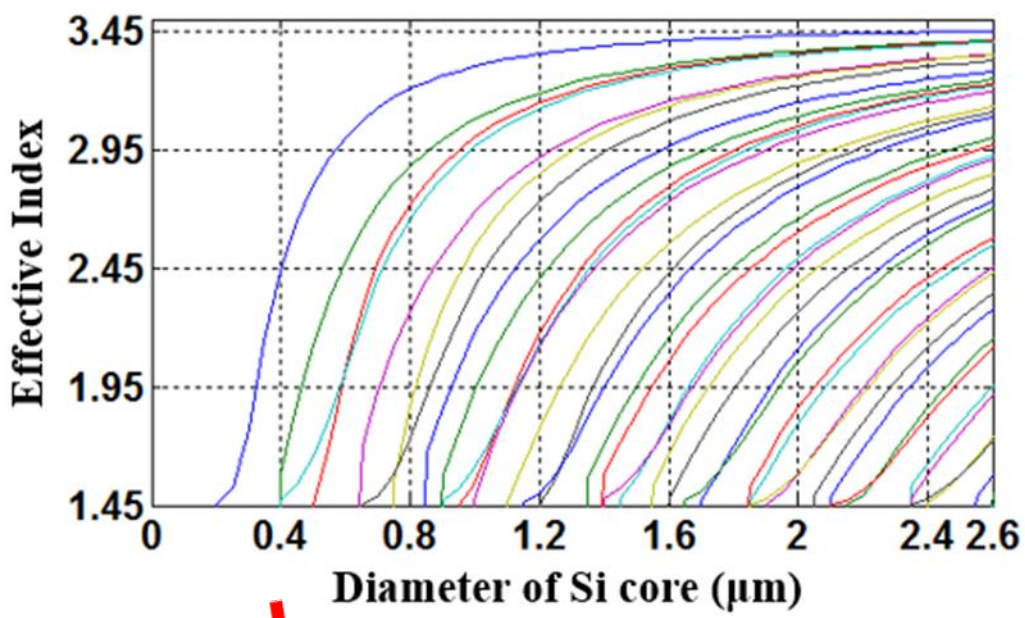
Fig. 3-9 (Top)The effective indices of different modes of Si-cored tapered fiber smaller than 2.6 μm in diameter at the wavelength of 1550 nm. (Bottom)Enlarged diagram for clearly indicating the single-mode operation region.

3.3.2   Loss Measurement of Silicon-Cored Tapered Fibers

We measured the transmission losses of the Si-cored tapered fibers and the picture of measurement setup is shown in Fig. 3-10. Light at a wavelength of 1550 nm was launched from a tunable laser diode (LUNA Phoenix 1400) through a lead-in silica tapered fiber (focused spot size ~2.5 x 2.4 μm) into a Si-cored tapered fiber. The optical coupling was monitored by using two charge-coupled device cameras from side- and top-view to ensure that the light was precisely delivered to the Si-cored tapered fiber. The transmitted light was then focused by an objective (Edmund Optics, 40x, NA=0.65), finally collected by a power detector. A series of output power in a function of input power is shown in Fig. 3-11. The total device loss is large (~30 dB). We estimated that this loss is most likely caused by reflection loss between air and Si, transmission loss with smaller diameter (~2.6 μm), end-face scattering loss without polishing process on fiber end-face and a non-adiabatic taper transition for the higher order modes [36].
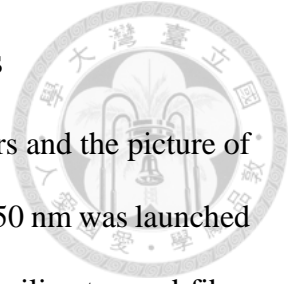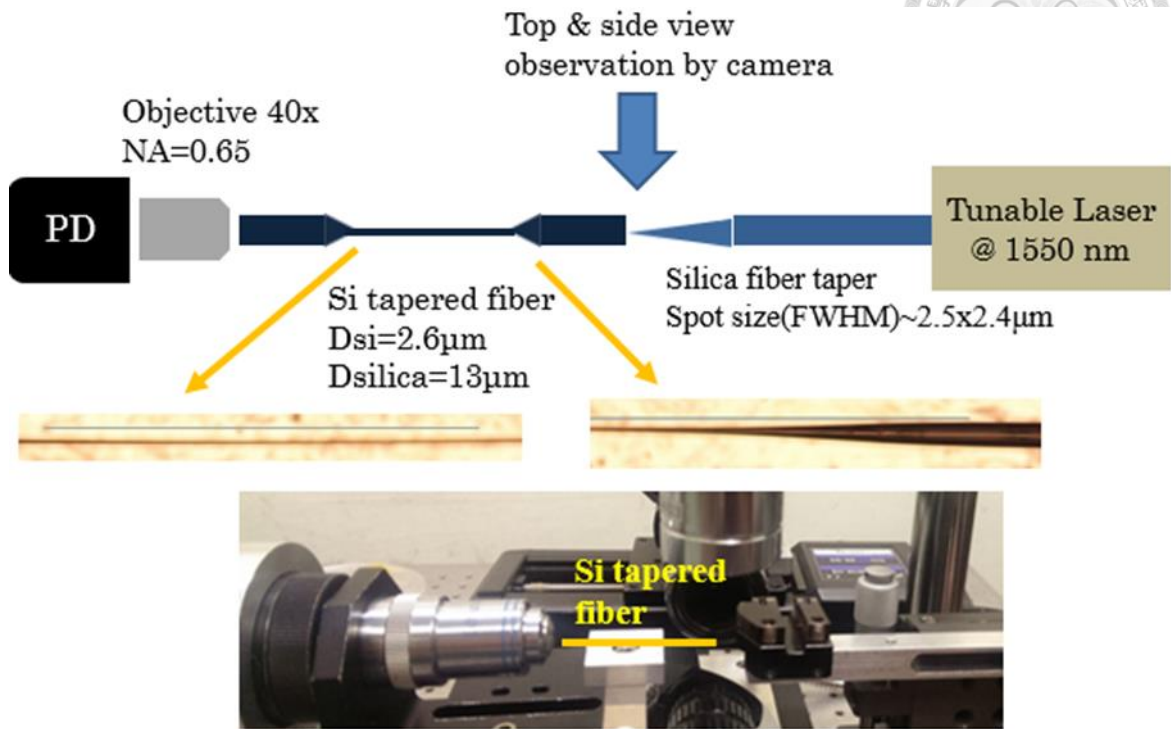
Fig. 3-10 A schematic diagram and a picture of transmission loss measurement setup.
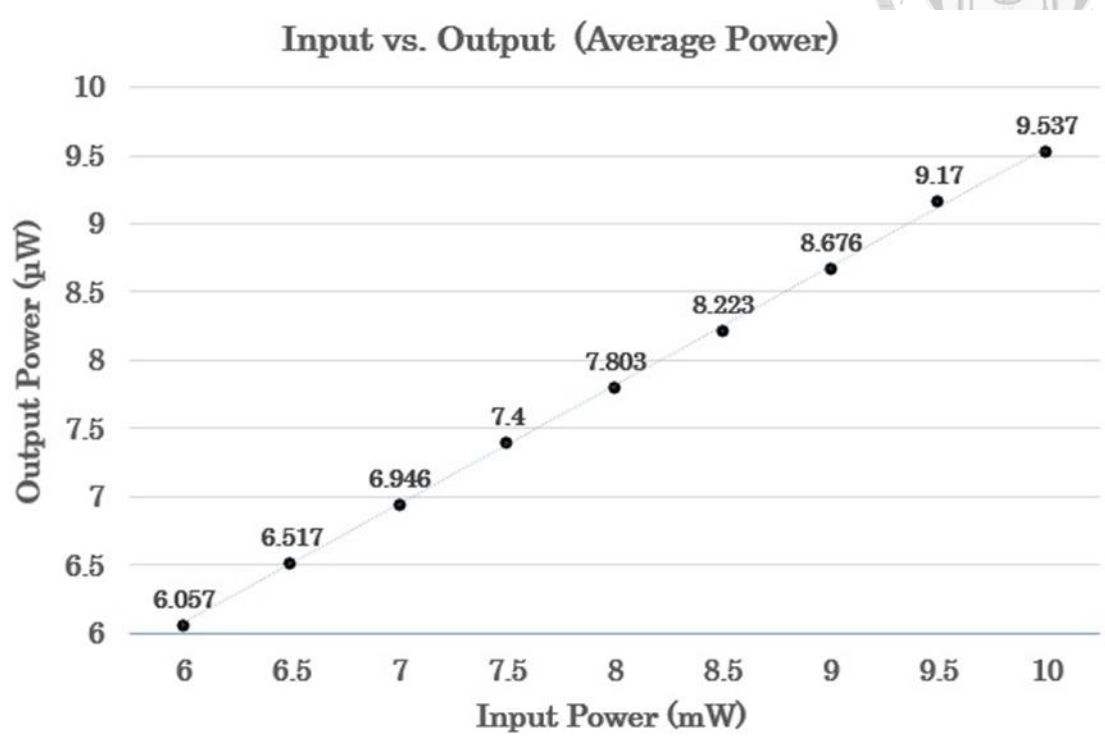
Fig. 3-11 A series of average output power in a function of average input power.

3.4 Summary

In this chapter, we have demonstrated a fiber drawing system for fabricating Si cored tapered fiber. A fiber drawing system equipped with oxy-hydrogen flame and transition stage was used. According to the previously rich knowledge in fabrication of silica microfiber, we successfully fabricated the Si cored tapered fiber with a diameter of 2.6 μm in the waist section from an original starting diameter of 20 μm. The total device loss was estimated to be caused by interface reflection and non-adiabatic taper transition, and we believed that it could be reduced by splicing of Si-core and silica single mode fiber and lengthening of taper region. Owing to its ease and versatility of this technique and the proof of enhancement of nonlinearity with smaller core dimension in past report [38], we expect Si cored tapered fiber could find wide applications in the Si photonics devices.

Chapter 4 Theory, Fabrication and Optical Characteristics of Silicon Microsphere Whispering Gallery Modes Resonator

4.1 Theory of Whispering Gallery Modes

4.1.1 Introduction of Whispering Gallery Modes

The modes of a spherical dielectric particle were first investigated by Mie at the beginning of the 19th century, in the context of light scattering from spherical particles. The scattering spectrum exhibited sharp features, which can be attributed to resonant circulation of optical energy within the sphere. These optical modes are confined by continuous total internal reflection at the dielectric air interface and are often referred to as whispering-gallery modes (WGMs). This description originated from the "problem of the whispering-gallery" which Lord Rayleigh published in 1912 [52], describing the phenomenon of acoustical waves he had observed propagating around the interior gallery of the Saint Paul's Cathedral, as shown in Fig. 4-1(a) and (b). A concept of WGMs in a microsphere is explained by geometry and wave optics respectively in Fig. 4-2(a) and (b). In the following sections, the resonant characteristics of microsphere, such as their field distribution, free spectral range, loss mechanism etc. are discussed in details.

(a)
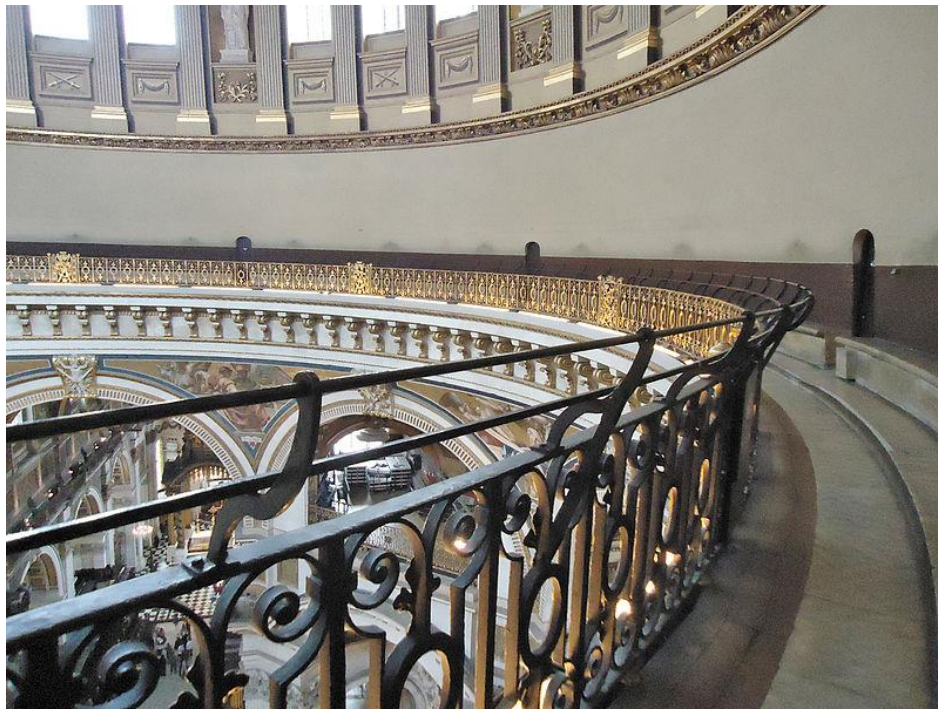
(b)

Fig. 4-1 (a) The interior dome of St Paul's Cathedral. (b) The Whispering Gallery of St Paul's Cathedral.
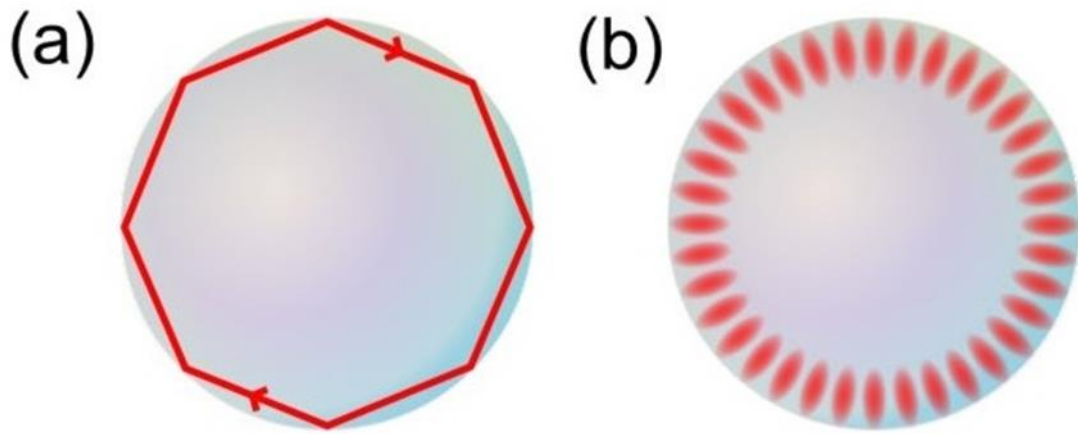
Fig. 4-2 (a) Geometry optics and (b) wave optics presentation of a WGMs.

(Pictures from "Soft Matter Laboratory")

4.1.2 Optical Modes of Microsphere Resonator

The optical modes of a microsphere can be calculated by solving Helmholtz equation in spherical coordinates, which has been treated by several authors (in particular see reference [53] for a comprehensive overview). A significant simplification occurs if the sphere consists of a homogeneous material, and if the optical modes reflect with grazing incidence upon the sphere-air boundary, such that the polarization can be assumed to be constant along the optical trajectories. Under this assumption the optical modes can be solved by the scalar wave equation approximation and solutions fall into two classes, and are either electric in character (TM-case) or magnetic in character (TE-case). The field components can be expressed in terms of a single field components ($E\varphi$ for the TM-case or $H\varphi$ for the TE-case) and solutions are found by solving the scalar wave equation for either the E_φ or H_φ alone by the separation of variables approach, i.e. E_φ or $H_\varphi = \psi(\varphi, \theta, r) = \psi_\varphi(\varphi)\psi_\theta(\theta)\psi_r(r)$. TE modes possess an electric field is parallel to the surface of the sphere (i.e. $E_\varphi = E_r = 0$, i.e. $\vec{E} \parallel \vec{\theta}$),whereas the TM modes possess a magnetic field which is parallel to the surface of the sphere, i.e. (i.e. $H_\varphi = H_r = 0$, i.e. $\vec{H} \parallel \vec{\theta}$). As a result, the electric field distribution of TM modes is predominantly radial in character. The introduced eigenfunctions for the radial, azimuthal and polar fields can be associated with the radial mode number (n), the polar mode number (*l*) and the azimuthal mode number (m). The azimuthal eigenfunctions are given by:

$$\psi_\varphi = \frac{1}{\sqrt{2\pi}} e^{\pm i\omega t} \qquad (4.1)$$

By introducing the polar mode number *l*, the equation for ψ_θ is given by:

$$\frac{1}{\cos(\theta)}\frac{d}{d\theta}\left(\cos(\theta)\frac{d}{d\theta}\varphi_\theta\right) - \frac{m^2}{\cos(\theta)^2}\varphi_\theta + l(l+1)\varphi_\theta = 0 \quad (4.2)$$

And finally the radial field ψ_r has to obey:

$$\frac{d^2}{dr^2}\varphi_r + \frac{2}{r}\frac{d}{dr}\varphi_r + \left(k^2 n(r)^2 - \frac{l(l+1)}{r^2}\right)\varphi_r = 0 \qquad (4.3)$$

The last two equations possess analytical solutions in terms of the generalized Legendre Polynomials $P_m^l(\cos\theta)$ (which are commonly re-expressed as the spherical Harmonics $Y_m^l(\theta)$) and the Bessel functions $j_l(kr)$. For each polar mode number l, the allowed azimuthal mode numbers are in the range of $-l < \mathrm{m} < l$, leading to a $2l+1$ degeneracy of the azimuthal modes.

4.1.3 Quality Factor

The quality factor (Q) is a well-known parameter used to measure the ability of energy storage in a resonant cavity. The Q represents how long the photon time traveling in a resonant cavity before it losses all its energy. These loss mechanisms include surface scattering loss, material loss, coupling loss between resonator and waveguide etc. The Q is a numerically measure of the ratio of the energy stored in a resonator to the energy dissipated by the resonator after one cycle. It is represented by:

$$Q = \frac{energy\ stored\ in\ cavity}{energy\ dissipated\ after\ one\ cycle} \qquad (4.4)$$

Since the energy is in direct relation with the frequency or the wavelength of photons, the energy stored can be represented as the wavelength of the resonant mode wavelength. The energy dissipated after one cycle is representative of the broadening of the cavity mode, therefore, can be characterized by the width of the cavity mode. Hence, the Q can be derived as:

$$Q = \frac{\lambda}{\Delta\lambda} \qquad (4.5)$$

where λ is the resonant wavelength of the WGM, and Δλ is the full-width-half-maximum of the WGM.

4.2   Fabrication of Silicon Microsphere Resonator
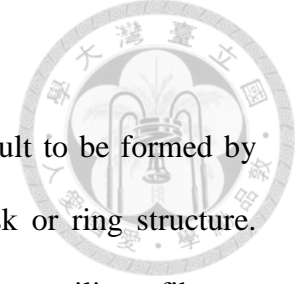
It is worth noting that a 3D sphere structure is relatively difficult to be formed by using standard semiconductor process in comparison with 2D disk or ring structure. Therefore, we adopted the CO_2 laser reformation method over a pure silicon fiber to fabricate a Si microsphere and the resonant characteristics will be reported elsewhere. The Si-cored fiber used in this work had been introduced in details in Chapter 2.

A Si-cored fiber manufactured by ourselves was used to fabricate Si microsphere, and the process details as shown in Fig. 4-3. In the first step, A part of silica cladding of Si-cored fiber was etched away by using hydrofluoric acid, and then immersed in a buffered oxide etch for confirming totally silica removing, and rinsed it in deionized water for cleaning after second etching. Careful control of etch time allowed us to release the Si core in a diameter of 21 μm from the silica cladding, as shown in Fig. 4-4(b). The released Si-core was exposed to a 10 W CO_2 laser beam (Synrad 48-series, λ=10.6μm) through a zinc-selenide lens (transmission at λ=10.6μm: >90%). To real-time monitor the fabrication process, a microscope equipped with a CCD camera was set up on top of the Si-core. By carefully adjusting the working distance of laser beam and laser output power, an appropriate heating temperature could be reached to ensure the successful fabrication of a Si microsphere as shown in Fig. 4-4(b), and Fig. 4-4(c) shows another bigger microsphere. The resultant diameter of microsphere was mainly dependent on the starting diameter of Si core. A Si microsphere was fixed on the end of the Si-cored fiber stem for easy handling and prevent its surface from being accidentally touched.

After the completion of Si microsphere by laser reformation, the Raman spectroscopy was applied to observe the difference between Si core and Si microsphere. Fig. 4-5 shows the Raman spectra of the Si core and the Si microsphere. The Raman peaks of the Si core and the Si microsphere are located at 517.9 cm^{-1} and 508.1 cm^{-1}, respectively. It is

apparent that the peak position is shifted to shorter wavenumbers after the laser exposure. We estimated the result of Raman shift is possibly induced by the effect of laser heating of the sample [54]. The Ref. 54 shows the Raman shift to shorter wavenumbers and broadening of spectrum width after laser heating, which are correspond to our result.
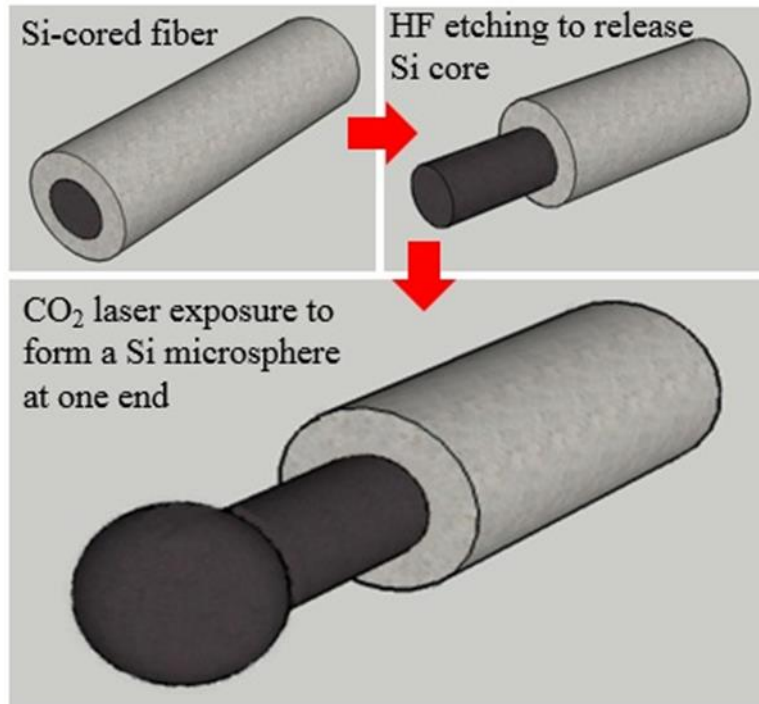
Fig. 4-3 Flow diagram illustrating the process details used to fabricate a Si microsphere resonator from a Si-cored fiber.
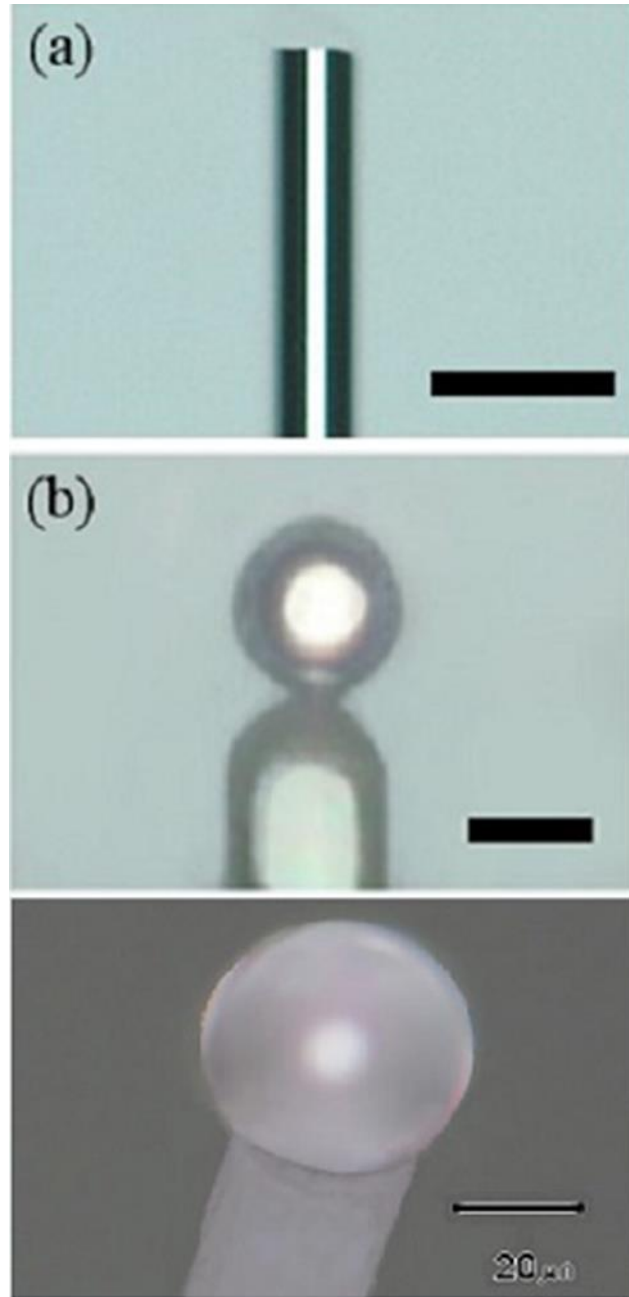
Fig. 4-4 Optical microscope pictures show that (a) a pure Si-core in diameter of 21 μm after chemical etching (scale bar: 50 μm) and (b) a completed Si microsphere in diameter of 14.6 μm fabricated by CO_2 laser reformation (scale bar: 10 μm), (c) a larger Si microsphere in diameter of 42 μm.
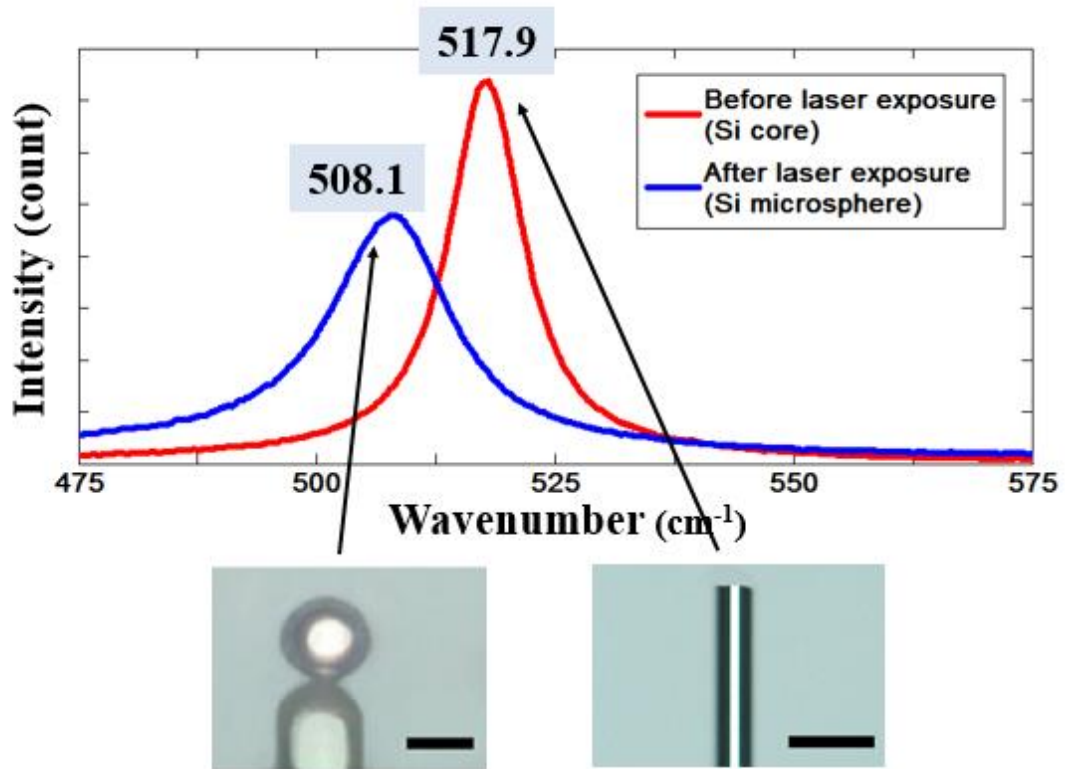
Fig. 4-5 Raman spectrum of Si core and Si microsphere.

4.3   Optical Characteristics of Silicon Microsphere Resonator

4.3.1   Tapered Fiber Coupling Method

The most commonly used coupling method to couple light into a microsphere is depicted in Fig. 4-6 [55]. It is based on evanescent-wave coupling either from an adjacent guiding structure such as (a) a tapered optical fiber and (b) a channel waveguide, or (c) from a prism, or (d) an angle-polished fiber under total internal reflection (TIR). The tapered fiber is an excellent and easily aligned coupling tool that allows fine tuning of the fiber mode propagation constant by controlling the taper diameter. Tapered fiber are commonly fabricated by heating and at the same time slowly pulling a section of the fiber to form a narrow waist. Advanced fiber splicing equipment or specific microfurnaces are used for this purpose. The appropriate taper waist can be as small as a micrometer in diameter, with the fundamental mode extending significantly into the free space surrounding the taper. The typical total length of the adiabatic tapered section is more than 1cm. A critical point for fiber couplers is the fact that the tapered region is very thin and therefore very fragile and easy to deteriorate.

The integrated waveguide coupler consists of a properly designed phase-matched surface-channel waveguide whose evanescent field overlaps with the microsphere WGMs. Achieving an efficient coupling is rather critical and requires a careful alignment, but the system is more compact and robust than the fiber taper.

Prism-to-sphere coupling is among the earliest concepts. A laser beam is directed into a prism and undergoes TIR at the prism surface. The resulting evanescent field at the prism surface can then be coupled into the microsphere. Phase matching is obtained by selecting the proper incidence angle. The system is rather robust, but achieving optimal

alignment is quite challenging.

The fiber-prism coupler combines the advantages of waveguide light insertion with the robustness of prism coupling. A fiber end is polished along a specific angle that allows phase matching. This angled plane then acts as a TIR surface for the light guided into the fiber that can thus be coupled to the microsphere. The fiber-prism method eliminates part of the alignment steps that are necessary for bulk prism couplers. It is worth noting that in the tapered fiber or waveguide coupling systems the transmitted light, after the interaction with the microsphere, is still conveniently guided into the same fiber or waveguide, while in the other approaches it propagates in free space.

Here, we adopted a tapered fiber as coupling tool due to its convenient control, high coupling efficiency and our past experiences [40]. The tapered fiber was fabricated from a standard single mode fiber by using the flame drawing technique, the fiber drawing tower we used had been discussed in Chapter 3, a photograph of fiber drawing tower and a scanning electron image of tapered fiber with diameter of ~1.14μm is shown in Fig. 4-7(a) and (b), respectively. The diameter of the tapered fiber smoothly varied from the original 125 μm to several microns in the waist section, whose propagation loss of a diameter of 3 μm could be measured as low as 0.0001 dB/mm when a tapered fiber was drawn at constant speed [49]. Fig. 4-8 shows the intensity profiles of fundamental modes of microfibers at the wavelength of 1550 nm with different diameters. The penetration lengths of evanescent fields expand when the diameters of microfibers decrease. This is the reason why the coupling efficiency increases with smaller diameter of microfiber. The experiment setup of measurement is shown in Fig. 4-9. The tapered fiber was placed on a 3-axis precision transition stage equipped with feedback system in order to precisely control the coupling gap between the tapered fiber and the Si microsphere for coupling optimization. A tunable continuous wave laser source (LUNA, Phoenix 1400) controlled

via a desktop computer was used to scan the wavelengths. An isolator was used to avoid the damage to the laser diode caused by the back-reflection from the Si microsphere. The output resonance spectrum was detected by using the built-in power detector of the laser source. Both scanning properties and the data acquisition system were controlled by using a user interface in a desktop computer.
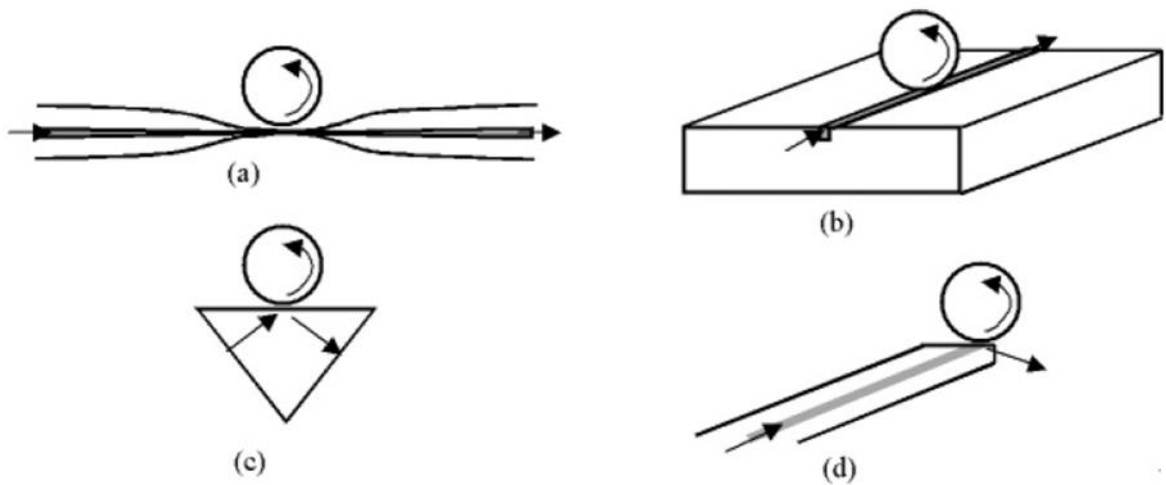
Fig. 4-6 Schemes of evanescent wave coupler used to inject light into a microsphere. (a) Tapered fiber, (b) integrated waveguide, (c) prism and (d) angle polished fiber [55].
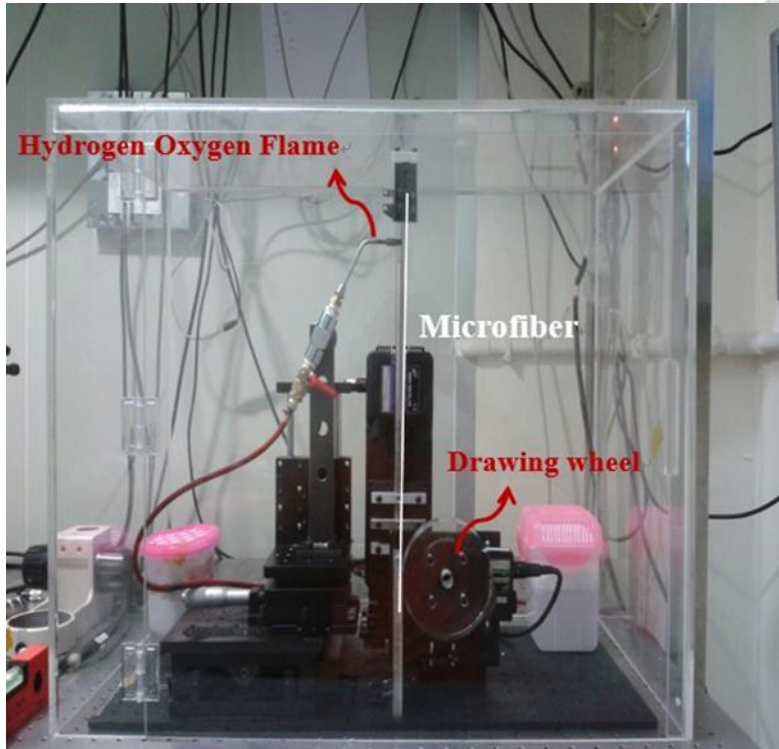
(a)
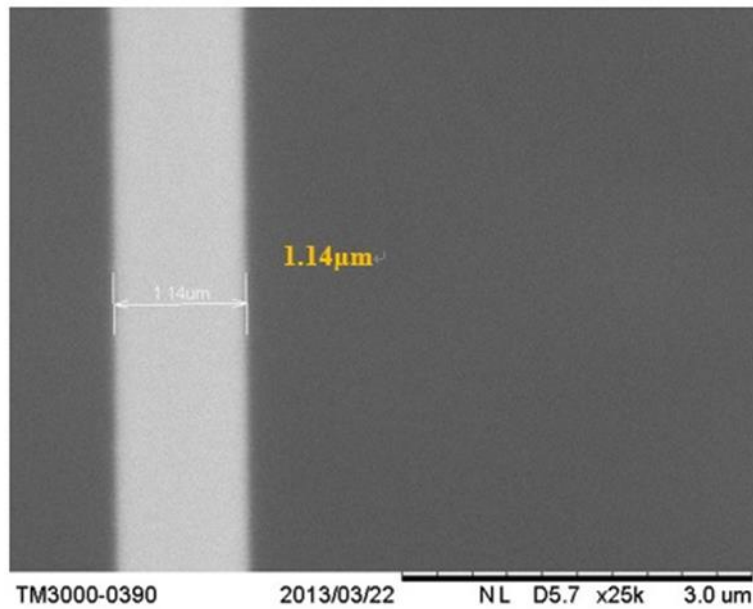
(b)

Fig. 4-7 (a) A photograph of a fiber drawing tower for making tapered fiber. (b) A scanning electron picture of tapered fiber with diameter of ~1.14 μm.
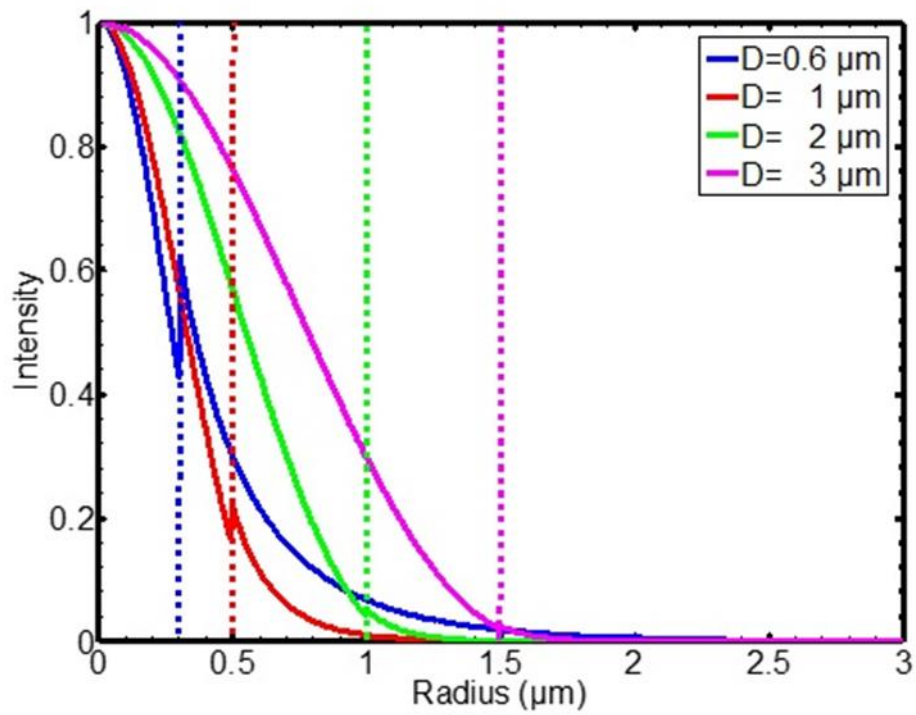
Fig. 4-8　The intensity profile of fundamental mode of microfibers at the wavelength of

1550 nm with different diameters depicted from the center. The dotted line is the boundary

between microfibers and air.
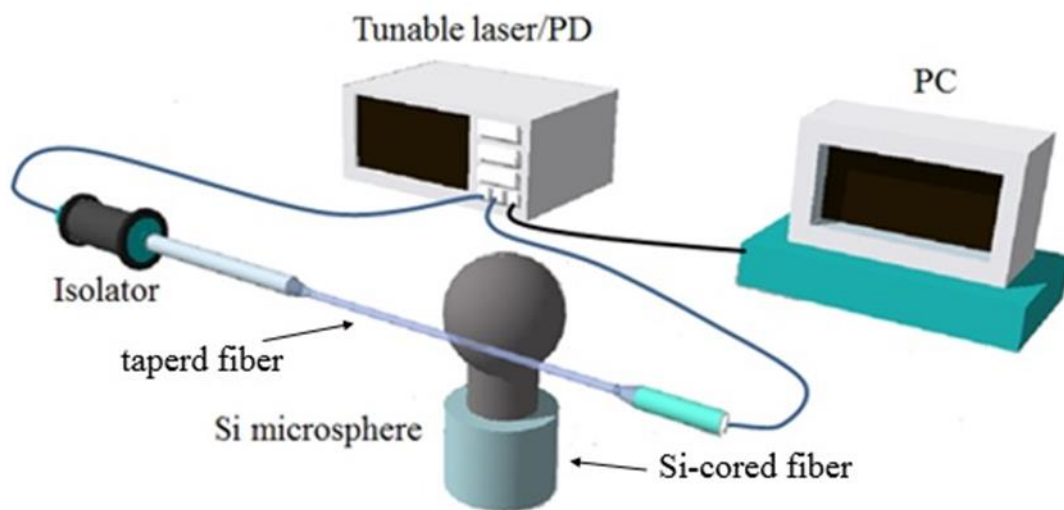
Fig. 4-9 Schematic diagram of tapered fiber coupling method. An isolator was used to avoid the damage to the laser diode caused by the back-reflection from the Si microsphere. A tapered fiber with diameter of ~1.5 μm in the waist section is employed to couple the light in and out.

4.3.2   Whispering Gallery Resonance in Silicon Microsphere

A tapered fiber in diameter of ~1.5 μm in the waist section was gradually approached a Si microsphere. As seen in Fig. 4-10, the normalized transmission spectrum ranging from 1520 to 1560 nm for a 14.6 μm diameter Si microsphere clearly shows the several resonant dips. The free spectral range was measured to be approximately 15.38 nm, which corresponds to a sphere diameter of 14.3 μm diameter based on the following relationship

$$\Delta\lambda_{\text{FSR}} = \frac{\lambda^2}{2\pi R n} \qquad\qquad (4.6)$$

where R is the radius of the microsphere, n is the refractive index of the Si (n~3.48) and λ is the dip position of wavelength. In spite of the large refractive index difference between the silica tapered fiber and the Si microsphere, the phase mismatching condition still can be overcame with small size of resonator and generations of high-order radial mode [56]. Moreover, it had already been achieved in other high refractive index microsphere through low index silica tapered fiber, such as chacolgenide glass (n~2.83) [57] and GaAs [58]. The normalized transmission spectrum measured for another microsphere is shown in Fig. 4-11(a), these resonant dips were loaded with average Q is ~2×10^5. Moreover, one of the resonant dip in Fig. 4-11(b) is located at wavelength of 1527.18 nm with a bandwidth Δλ of 3.72 nm. Therefore, the measured Q=λ/Δλ of this resonance is 4×10^5, which is the highest Q in this work. To our best knowledge, this is among the highest orders of Q achieved with high refractive index material by a lower refractive index waveguide like silica
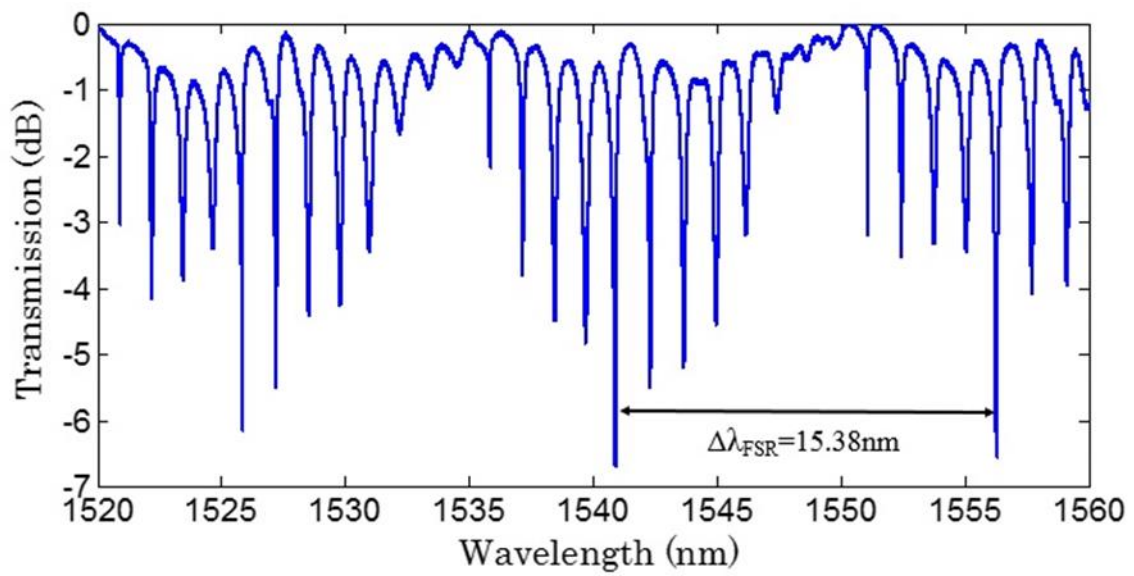
Fig. 4-10 The transmission spectrum for wavelengths ranging from 1520 to 1560 nm for a Si microsphere in diameter of 14.6 um, which corresponds to the measured FSR in spectrum.
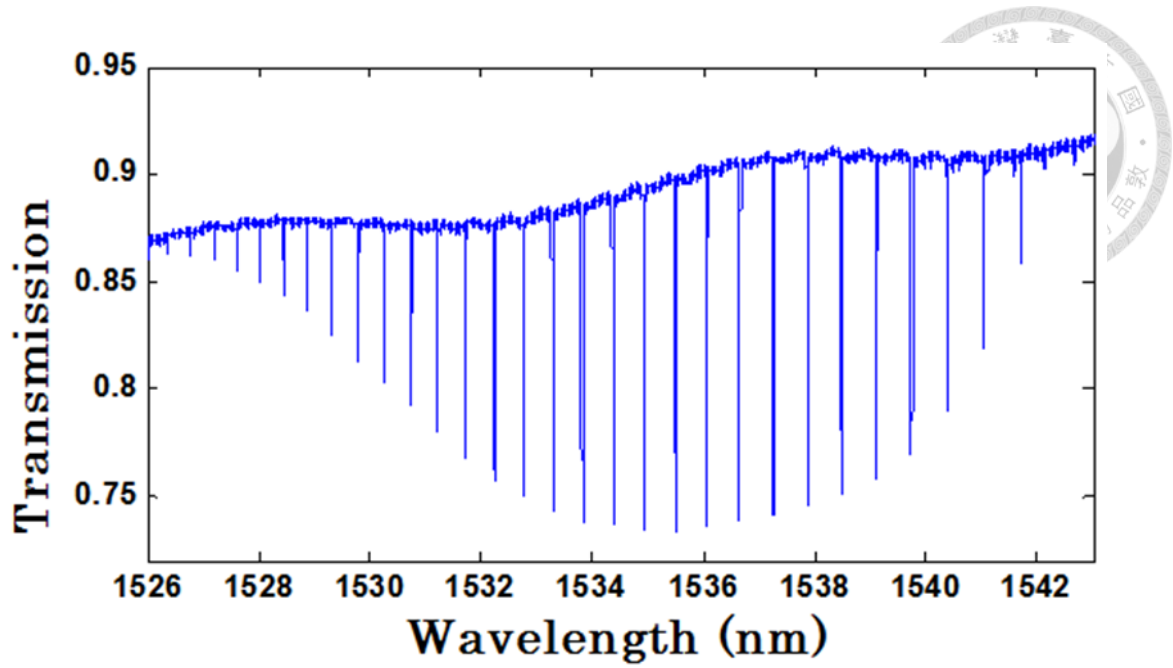
(a)
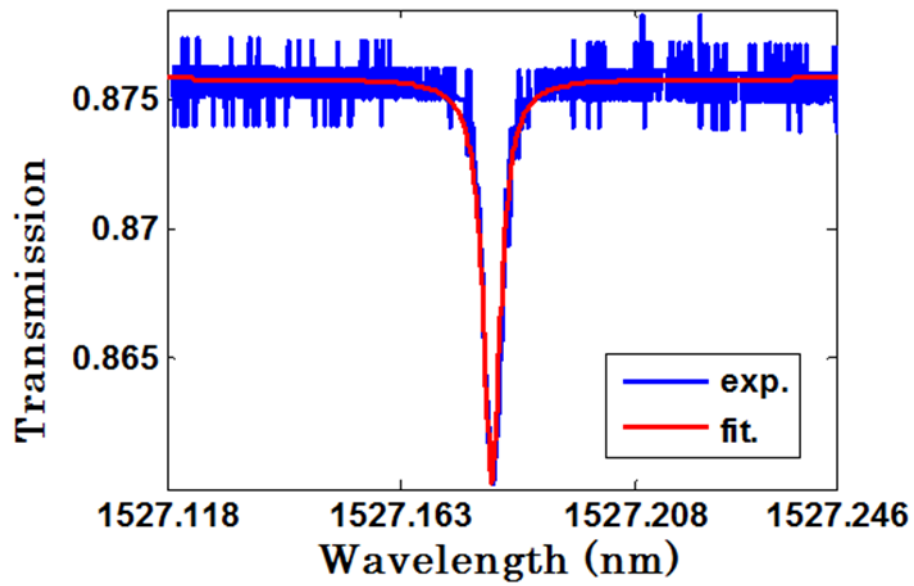
(b)

Fig. 4-11 (a) Normalized transmission spectrum for a 25.4 μm diameter Si microsphere with the highest resonant Q in this work. (b) The enlarged spectrum shows that a single resonant dip at wavelength of 1527.18 nm with the highest measured Q ~ 4 x 10^5 and the fitted Lorentzian curve.

4.3.3 Thermo-Optic Effect Induced by Absorption of Incident Power

The thermo-optic effect (TOE) is a well-known phenomenon in physics. It determines the variation of the refractive index of a material when a temperature change occurs. This effect has been extensively used in optoelectronics as well as in sensors technology for the realization of a large variety of devices, mostly based on interferometric principles, such as optical switches tunable filters, tunable lasers and fiber-optic sensors [59].

In order to characterize a material from the thermo-optic point of view, the thermo-optic coefficient $\Delta n/\Delta T$ is generally used. It has been highlighted [60] that among the common thermo-optical materials Si shows the highest coefficient, being in fact $\Delta n_{si}/\Delta T =$ 1.86 X 10^{-4} K^{-1} at the fiber optic wavelength of 1.55 μm, which is double the coefficient of $LiNbO_3$ and even 15-fold higher than in silica fiber.

We investigate this thermo-optic effect in Si microsphere resonator through adjusting the input power leading to the shift of resonant wavelength position. A set of power dependent experiments by scanning over the resonant wavelength at ~1551 nm, as shown in Fig. 4-12. From these results, it is evident that the position of resonant dip is moving to the longer wavelength region when the input power was increased from 6 to 10 mW step by step. The starting position of resonant wavelength is located at 1550.971 nm, which is rightly shifted for a range of 123 pm to be at 1551.095 nm when the input power was increased from 6 to 8 mW. And then, the position of resonant wavelength moves to be at 1551.111 nm when the input power was increased again from 8 to 10 mW. However, such increasing range of wavelength shift is relatively small in comparison with Si microcylindrical structure [18], which we attributed to the larger volume of sphere structure, therefore smaller change in refractive index of resonator in this work.
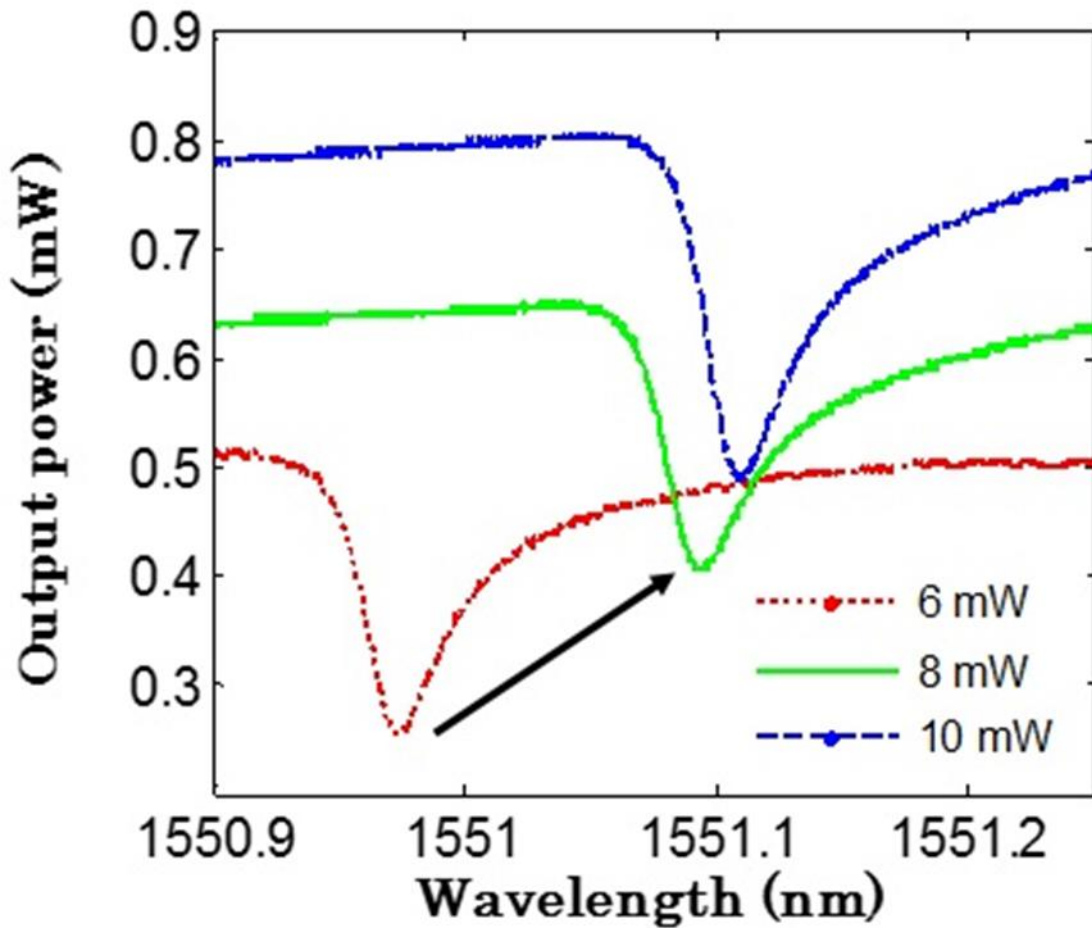
Fig. 4-12 The resonant wavelength shift induced by thermo-optic effect through gradually increasing the incident power from 6 to 10 mW. The arrow means the moving direction of wavelength shift.

4.4　Summary

A Si microsphere was fabricated by using CO_2 laser reformation method over a Si-cored fiber without silica cladding. A tapered fiber coupling method was adopted for coupling the evanescent wave into the Si microsphere and successfully excited the high Q WGM resonance. The WGM spectrum at telecommunication band was presented and obtained the highest $Q \sim 4 \times 10^5$ in sphere resonator achieved with high refractive index material by a lower refractive index silica waveguide. In addition, the thermo-optic effect of Si material has been demonstrated as we performed a set of input power dependent experiments through increasing input power. The temperature increase inside the resonator due to the absorption of power coupled into the Si microsphere led to a wavelength shift induced by a change of refractive index in the Si microsphere. This chapter describes a simple and effective method to achieve a high Q resonator in Si material instead of time-consuming standard semiconductor process.
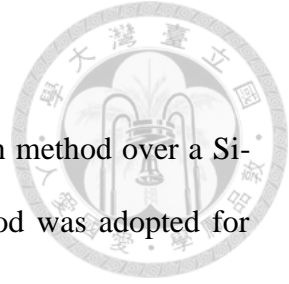
Chapter 5   Conclusions and Future Work

5.1   Conclusion

In this thesis work, we successfully demonstrate Si-cored fibers with single crystalline state, lower transmission loss in telecommunication band, meter-long and uniform dimension in core and cladding by using a combined technique of rapid-drawing and powder-in-tube. Moreover, a novel method has been presented to fabricate a Si microsphere resonator from a Si-cored fiber by using CO_2 laser reformation process. WGM in a Si microsphere resonator has been obtained with Q as high as 4×10^5. To our best knowledge, such Q from a Si spherical resonator by using a silica tapered fiber for coupling is the highest as compared to the existing literature. We believe this Si resonator with high Q may find useful applications in sensing and nonlinear optics.

In addition to Si microsphere demonstration, a potential work about Si-cored tapered fibers is also highlighted in this thesis. As introduced in Chapter 3, Si-cored tapered fibers were fabricated from Si-cored fibers by using a miniaturized fiber drawing tower. A Si-cored fiber of diameter 20 µm is heated by a hydro-oxygen flame and then rapidly drawn downward in order to form taper shape, resulting the core diameter as small as ~ 2.6 µm. The resultant Si-cored tapered fiber has a total device loss ~ 30 dB, which is attributed to interface reflection at both end, transmission loss of smaller core diameter, end-face surface scattering loss and non-adiabatic taper transition.

5.2   Future Work

According to the previous report [38], the optical nonlinearities like Kerr effect can be greatly enhanced after the shrinkage in cross-section area of waveguide. Furthermore, the number of guided modes in the Si-core could be effectively reduced the Si-cored tapered fiber with smaller dimension. This fabrication method of tapered fiber can be used to provide a possibility for demonstrating single-mode transmission in Si-cored fiber, implying the application of nonlinear optics using Si-cored tapered fibers is promising in future work.

We believe that the Si WGM resonators with high Q's have an opportunity of being good active elements according to the past reports on Raman effect in Si material. For example, a demonstration of all-Si Raman lasing experiment involving Si as the gain medium using stimulated Raman scattering has been reported [61]. Based on the high nonlinearities in Si and WGMs resonance with high-Q, Si WGMs resonators serve good candidates as amplifier or laser.
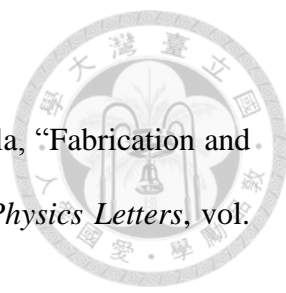
Next, let's focus on sensing. Based on early reports, the detection limit is proportional to the quality factor [62]. The higher quality factor of WGM resonators, the sharper dips of spectra at resonant wavelength and the smaller amount of shift of resonant wavelength can be distinguished. So only if the quality factor of resonator is high enough, the low detection limit can be achievable. The good transmission spectral feature of Si at mid-infrared region is promising for bio-sensing and chemical sensing. Some reports on Si devices for bio-sensing and chemical sensing at mid-infrared region have been published [63][64].
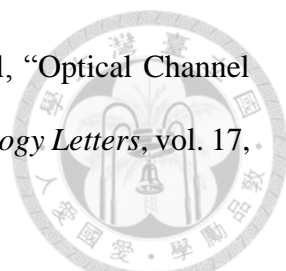
References
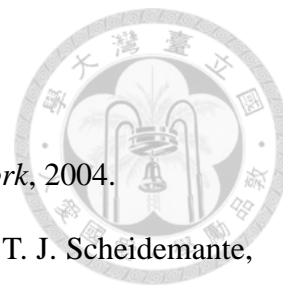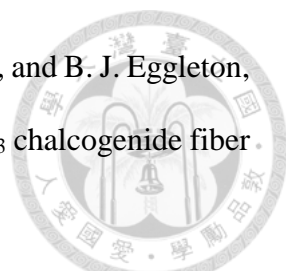
[1] G. T. Reed, and A. P. Knights, "Silicon Photonics," *Wiley New York*, 2004.

[2] P. J. A. Sazio, A. Amezcua-Correa, C. E. Finlayson, J. R. Hayes, T. J. Scheidemante, N. F. Baril, B. R. Jackson, D. J. Won, F. Zhang, E. R. Margine, V. Gopalan, V. H. Crespi, J. V. Badding, "Microstructured Optical Fibers as High-Pressure Microfluidic Reactors," *Science*, vol. 311, pp. 1583–1586, 2006.

[3] P. Mehta, N. Healy, N. F. Baril, P. J. A. Sazio, J. V. Badding, and A. C. Peacock, "Nonlinear transmission properties of hydrogenated amorphous silicon core optical fibers," *Optics Express*, vol. 18, pp. 16826-16831, 2010.

[4] L. Shen, N. Healy, P. Mehta, T. D. Day, J. R. Sparks, J. V. Badding, and A. C. Peacock, "Nonlinear transmission properties of hydrogenated amorphous silicon core fibers towards the mid-infrared regime," *Optics Express*, vol. 21, pp.13075-13083, 2013.

[5] N. Vukovic, N. Healy, P. Mehta, T. D. Day, P. J. A. Sazio, J. V. Badding, and A. C. Peacock, "Thermal nonlinearity in silicon microcylindrical resonators," *Applied Physics Letters*, vol. 100, pp. 181101-1 − 181101-4, 2013.

[6] A. B. Matsko and V. S. Ilchenko, "Optical Resonators With Whispering-Gallery Modes—Part I: Basics," *IEEE Journal of Selected Topics in Quantum Electronics*, vol. 12, pp. 3-13, 2006.

[7] V. S. Ilchenko and A. B. Matsko, "Optical Resonators With Whispering-Gallery Modes—Part II: Applications, " *IEEE Journal of Selected Topics in Quantum Electronics,* vol. 12, pp. 15-32, 2006.

[8] K. J. Vahala, "Optical Microcavities," *Nature,* vol. 424, pp. 839-846, 2003.

[9] M. Cai, O. Painter, and K. J. Vahala, "Observation of Critical Coupling in a Fiber Taper to a Silica-Microsphere Whispering-Gallery Mode System," *Physical Review*

Letters, vol. 85, pp. 74-77, 2000.
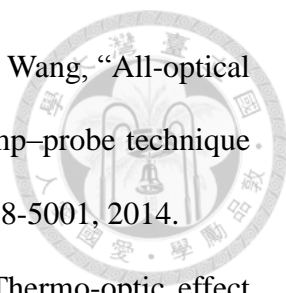
[10] T. J. Kippenberg, S. M. Spillane, D. K. Armani, and K. J. Vahala, "Fabrication and coupling to planar high-Q silica disk microcavities," *Applied Physics Letters*, vol. 83, pp. 797-799, 2003.

[11] D. K. Armani, T. J. Kippenberg, S. M. Spillane & K. J. Vahala, "Ultra-high-Q toroid microcavity on a chip," *Nature*, vol. 421, pp. 925-928, 2003.

[12] F. Vollmer, D. Braun, A. Libchaber, M. Khoshsima, I. Teraoka, and S. Arnold, "Protein detection by optical shift of a resonant microcavity," *Applied Physics Letters,* vol. 80, pp. 4057-4059, 2002.

[13] Y. F. Xiao, C. H. Dong, C. L. Zou, Z. F. Han, L. Yang, and G. C. Guo, "Low-threshold microlaser in a high-Q asymmetrical microcavity," *Optics Letters*, vol. 34, pp. 509-511, 2009.

[14] Faraz Monifi, S. K. Ozdemir, and L. Yang, "Tunable add-drop filter using an active whispering gallery mode microcavity," *Applied Physics Letters,* vol. 103, pp. 181103-1 − 181103-4, 2013.

[15] O. Boyraz and B. Jalali, "Demonstration of a silicon Raman laser," *Optics Express*, vol. 12, pp. 5269-5274, 2004.

[16] M. Soltani, S. Yegnanarayanan and A. Adibi, "Ultra-high Q planar silicon microdisk resonators," *Optics Express,* vol. 15, pp. 4694-4704, 2007

[17] H, Yi, D. S. Citrin, and Z. Zhou, "Highly sensitive silicon microring sensor with sharp asymmetrical resonance," *Optics Express*, vol. 18, pp. 2967-2972, 2010.

[18] N. Vukovic, N. Healy, P. Horak, J. R. Sparks, P. J. A. Sazio, J. V. Badding, and A. C. Peacock, "Ultra-smooth microcylindrical resonators fabricated from the silicon optical fiber platform," *Applied Physics Letters*, vol. 99, pp. 031117-1 − 031117-3, 2011.

[19] Y. O. Yilmaz, A. Demir, Student, A. Kurt, and A. Serpengüzel, "Optical Channel Dropping With a Silicon Microsphere," *IEEE Photonics Technology Letters*, vol. 17, pp. 1662–1664, 2005.

[20] E. Yüce, O. Gürlü, and A. Serpengüzel,, "Optical Modulation With Silicon Microspheres," *IEEE Photonics Technology Letters,* vol. 21, pp. 1481-1483, 2009.

[21] J. Ballato, T. Hawkins, P. Foy, R. Stolen, B. Kokuoz, M. Ellison, C. McMillen, J. Reppert, A. M. Rao, M. Daw, S. Sharma, R. Shori, O. Stafsudd, R. R. Rice, and D. R. Powers," Silicon optical fiber," *Optics Express*, vol. 16, pp. 18675-18683, 2008.

[22] B. Scott, K. Wang, V. Caluori, and G. Pickrell, "Fabrication of silicon optical fiber," *Optical Engineering Letters*, vol. 48, pp. 100501-1 − 100501-3, 2009

[23] W. R. Mckee, "Development of the Spherical Silicon Solar Cell," *IEEE Transactions on Components, Hybrid, and Manufacturing Technology*, vol. CHMT-5, pp. 336-341, 1982.

[24] K.C. Kao and G.A. Hockham, "Dielectric-fibre surface waveguides for optical frequencies," *IEEE Proceedings*, vol. 133, pp. 191-198, 1986.

[25] D. J. Gardiner, P. R. Graves, H. J. Bowley , D. L. Gerrard, J. D. Louden, G. Turrell, "Practical Raman Spectroscopy," *Springer-Verlag,* 1989
optical frequencies," *IEEE Proceedings*, vol. 133, pp. 191-198, 1986.

[26] D. J. Won, M. O. Ramirez, H. Kang, V. Gopalana, N. F. Baril, J. Calkins, J. V. Badding, and P. J. A. Sazio, "All-optical modulation of laser light in amorphous silicon-filled microstructured optical fibers," *Applied Physics Letters*, vol. 91, pp. 161112-1 − 161112-3, 2007.

[27] Y. Okada and Y. Tokumaru, "Precise determination of lattice parameter and thermal expansion coefficient of silicon between 300 and 1500 K," *Journal of Applied Physics*, vol. 56, pp. 314-320, 1984.

[28] B. H. W. S. D. Jong, R. G. C. Beerkens, P. A. V. Nijnatten, "Ullmann's encyclopedia of industrial chemistry," *Wiley, VCH*, 2000.

[29] F. Sugimoto and Y. Arimoto, "Bond Strength of Bonded SOI Wafers," *Japanese Journal of Applied Physics*, vol. 31, pp. 975-978, 1992.

[30] D. Liang, A. W. Fang, H. Park, T. E. Reynolds, K. Warner, D. C. Oakley, and J. E. Bowers, "Low-Temperature, Strong SiO_2-SiO_2 Covalent Wafer Bonding for III–V Compound Semiconductors-to-Silicon Photonic," *Journal of Electronic Materials,* vol. 37, pp. 1552-1559, 2008

[31] J. Goldstein, D. E. Newbury, D. C. Joy , C. E. Lyman, P. Echlin, E. Lifshin, L. Sawyer, J.R. Michael, "*Scanning electron microscopy and x-ray microanalysis*," *Springer,* 2003.

[32] S. Morris, T. Hawkins, P. Foy, J. Hudson, L. Zhu, R. Stolen, R. Rice, and J. Ballat, "On loss in silicon core optical fibers," *Optical Materials Express*, vol. 2, pp. 1511-1519, 2012.

[33] A. Ghata, and K. Thyagarajan "An introduction to fiber optics," ,1986.

[34] N. Vukovic, N. Healy, P. Mehta, T. D. Day, P. J. A. Sazio, J. V. Badding, and A. C. Peacock, "Thermal nonlinearity in silicon microcylindrical resonators," *Applied Physics Letters*, vol. 100, pp. 181101-1 – 181101-4, 2012.

[35] L. Lagonigro, N. Healy, J. R. Sparks, N. F. Baril, P. J. A. Sazio, J. V. Badding, and A. C. Peacock, "Low loss silicon fibers for photonics applications," *Applied Physics Letters*, vol. 96, pp. 041105-1 – 041105-3, 2010 .

[36] N. Healy, J. R. Sparks, P. J. A. Sazio, J. V. Badding, and A. C. Peacock, "Tapered silicon optical fibers," *Optics Express*, vol. 18, pp. 7596-7601, 2010.

[37] V. R. Almeida, R. R. Panepucci, and M. Lipson, "Nanotaper for compact mode conversion," *Optics Letters*, vol. 28, pp. 1302-1304, 2003.

[38] E. C. Mägi, L. B. Fu, H. C. Nguyen, M. R. E. Lamont, D. I. Yeom, and B. J. Eggleton, "Enhanced Kerr nonlinearity in sub-wavelength diameter As_2Se_3 chalcogenide fiber tapers," *Optics Express*, vol. 15, pp. 10324-10329, 2007.

[39] A. Sure, T. Dillon, J. Murakowski, C. Lin, D. Pustai and D. W. Prather, "Fabrication and characterization of three-dimensional silicon tapers," *Optics Express*, vol. 11, pp. 3555-3561, 2003.

[40] 卓士閔, "將光纖抽絲塔微小化以製作微奈米導光線與其應用, Fabrication of Micro/Nano Optical Wires Using the Miniaturization of Fiber Drawing Tower and Their Applications," *Doctoral Dissertation,* 2012.

[41] L. L. Jr. Blyler, F. V. DiMarcello, "Fiber drawing, coating, and jacketing," *Proceedings of the IEEE*, vol. 68, pp. 1194-1198, 1980.

[42] U. C. Paek, "High-speed High-Strength Fiber Drawing," *Journal of Lightwave Technology*, vol. LT-4, pp. 1048-1060, 1986.

[43] U. C. Paek, "Free drawing and polymer coating of silica glass optical fibers," *Journal of Heat Transfer*, vol. 121, pp. 774-788, 1999.

[44] U. C. Paek and R. B. Runk, "Physical behavior of the neck-down region during furnace drawing of silica fibers," *Optical Fiber Transmission*, pp. TuCl-1 – TuCl-4, 1977.

[45] K. Imoto, M. Sumi, G. Toda, and T. Suganuma, "Optical Fiber Drawing Method with Gas Flow Controlling System," *Journal of Lightwave Technology*, vol. 7, pp. 115-121, 1989.

[46] S. Sakaguchi, and T. Kimura, "High-speed drawing of optical fibers with pressurized coating," *Journal of Lightwave Technology*, vol. LT-3, pp. 669-673, 1985.

[47] P. L. Chu, T. Whitbread, and P. M. Allen, "An on-line fiber drawing tension and diameter measurement device," *Journal of Lightwave Technology,* vol. 7, pp. 255-

261, 1989.

[48] C. G. Askins, M. A. Putnam, and E. J. Friebele, "Noncontact measurement of optical fiber draw tension," *Journal of Lightwave Technology*, vol. 9, pp. 945-947, 1991.

[49] T. H. Shen and L. A. Wang, "A Two-Layer Microcoil Resonator With Very High Quality Factor," *IEEE Photonics Technology Letters*, vol. 26, pp. 535-537, 2014.

[50] C. Tsao, "oprical fibre waveguide analysis," *Oxford University Press*, 1992.

[51] L. Tong, J. Lou, and E. Mazur, "Single-mode guiding properties of subwavelength-diameter silica and silicon wire waveguides," *Optics Express*, vol. 12, pp. 1025-1035, 2004.

[52] L. Rayleigh, "The problem of the whispering gallery," *Scientific Papers*, vol. 5, pp. 617-620, 1912.

[53] A. N. Oraevsky, "whispering-gallery waves," *Quantum Electronics*, vol. 32, pp. 377-400, 2002.

[54] X. M. Wua, J. Y. Yuc, T. L. Rena, L. T. Liua, "Micro-Raman spectroscopy measurement of stress in silicon," *Microelectronics Journal*, vol. 38, pp. 87-90, 2007.

[55] A. Chiasera, Y. Dumeige, P. F´eron, M. Ferrari, Y. Jestin , G. N. Conti, S. Pelli, S.Soria, and G. C. Righini, "Spherical whispering-gallery-mode microresonators," *Laser and Photonics Reviews*, vol. 4, pp. 457-482, 2010.

[56] J. C. Knight, G. Cheung, F. Jacques, and T. A. Birks, "Phase-matched excitation of whispering-gallery-mode resonances by a fiber taper," *Optics Letters,* vol. 22, pp. 1129-1131, 1997.

[57] C. Grillet, S. N. Bian, E. C. Magi, and B. J. Eggleton, "Fiber taper coupling to chalcogenide microsphere modes," *Applied Physics Letters*, vol. 92, pp. 171109-1 – 171109-3, 2008.

[58] Y. C. Lin, M. H. Mao, Y. R. Lin, H. H. Lin, C. A. Lin, and L. A. Wang, "All-optical switching in GaAs microdisk resonators by a femtosecond pump–probe technique through tapered-fiber coupling," *Optics Letters*, vol. 39, pp. 4998-5001, 2014.

[59] G. Cocorullo, F. G. D. Cart, I. Rendina, and P. M. Sarro, "Thermo-optic effect exploitation in silicon rnicrostructures," *Sensor and Actuators A*, vol. 71, pp. 19-26, 1998.

[60] G. Cocorullo, and I. Rendina "Thermo-optical modulation at 1.5 μm in silicon etalon," *Electronics Letters*, vol. 28, pp. 83-85, 1992.

[61] H. Rong, A. Liu, R. Jones, O. Cohen, D. Hak, R. Nicolaescu, A. Fang, and M. Paniccia, "An all-silicon Raman laser," *Nature*, vol. 433, pp. 292-294, 2005.

[62] C. Y. Chao, and L. J. Guo, "Design and optimization of microring resonators in biochemical sensing applications," *Journal of Lightwave Technology*, vol. 24, pp. 1395-1402, 2006.

[63] K. De Vos, I. Bartolozzi, E. Schacht, P. Bienstman, and R. Baets, "Silicon-on-Insulator microring resonator for sensitive and label-free biosensing," *Optics Express*, vol. 15, pp. 7610-7615, 2007.

[64] Y. Huang, S. K.Kalyoncu, Q. Zhao, R. Torun, O. Boyraz, "Silicon-on-sapphire waveguides design for mid-IR evanescent field absorption gas sensors," *Optics Communications*, vol. 313, pp. 186-194, 2013.